INT. REVIEWS IN PHYSICAL CHEMISTRY, 2003
VOL. 22, NO. 2, 221–262

Taylor & Francis
Taylor & Francis Group

Current understanding of the structure, phase transitions and dynamics of self-assembled monolayers on two- and three-dimensional surfaces

N. SANDHYARANI† and T. PRADEEP*

Department of Chemistry and Regional Sophisticated Instrumentation Centre, Indian Institute of Technology Madras, Chennai, 600 036 India

Self-assembled monolayers (SAMs) have been the preferred material systems to investigate specific properties in several disciplines for nearly 15 years. Advances in various techniques and their application to the study of SAMs have dramatically improved our understanding of these systems. Adaptation of this molecular architecture into three dimensions in the form of monolayer-protected clusters enabled the use of bulk techniques for the study of monolayers. Here we review recent developments in the structural properties and temperature-induced phase transitions of both these SAM structures. While alkanethiols on Au (111) and Ag (111) are taken as archetypal systems to discuss the properties of SAMs on two-dimensional surfaces, their assemblies on Au and Ag cluster surfaces are taken as examples for SAMs on three-dimensional surfaces. A comparison of these two SAMs is provided.

Contents

† Currently at Cornell University, Ithaca, New York.
* Author to whom correspondence should be addressed. E-mail: pradeep@iitm.ac.in

International Reviews in Physical Chemistry ISSN 0144–235X print/ISSN 1366–591X online © 2003 Taylor & Francis Ltd
http://www.tandf.co.uk/journals
DOI: 10.1080/0144235031000069705

1. Introduction

The fact that ultrathin films at interfaces determine surface properties such as friction and lubrication has been recognized for well over a century. The concept of monolayers was proposed by Irving Langmuir in 1917 while looking at the properties of amphiphiles on water [1]. He realized that amphiphilic films spread on water have a thickness of one molecule [1], although there have been earlier

reports on such a possibility [2, 3]. An ordered monolayer could be produced by applying pressure on a floating film [4]. Later, Katherine Blodgett succeeded in transferring these films to a solid surface [5]. These became known as Langmuir–Blodgett films. In spite of the wide application of these films, they are thermodynamically unstable and their formation requires specialized apparatus.

Spontaneous growth of monolayers was suggested by Zisman and coworkers in 1946 [6]. They observed that alkyl amines adsorb on platinum and spontaneous formation of an ordered monolayer results. These are known as self-assembled monolayers (SAMs) as their formation does not require any external pressure. SAMs are defined as ordered molecular assemblies formed by the spontaneous adsorption of an active surfactant on a solid surface. At that time, the potential of SAMs was not recognized. In 1983 Nuzzo and Allara showed that SAMs of alkanethiolates on gold could be prepared by the adsorption of *n*-alkyl disulphides from their dilute solutions [7]. Followed by this report, an exponential growth was observed in the field of SAMs. Various number of adsorbate–adsorbent combinations have been found [8, 9]. Among these, alkanethiol monolayers on coinage metals, especially on gold, became the centre of attraction because of the inertness of gold and the strong Au–S bond [10]. The ability to tailor the monolayer–air interface makes SAMs ideal model systems for studies of interfacial phenomena. Potential applications of these systems include sensors [11], corrosion inhibitors [12], molecular recognition [13] and molecular crystal growth [14]. Real applications of these systems require precise control of structural features and Allara's review describes the critical issues in the application of SAMs [15]. The number density of molecules on the surface is less ($\sim 10^{15}$ molecules per square centimetre of the surface) which makes it difficult to use conventional characterization techniques for their study. Therefore, it is necessary to increase the number of assembled molecules in the area of investigation; this is possible if the molecules are assembled on the surface of a nanocluster.

In 1994 Brust *et al*. reported the synthesis of monolayer-protected metal clusters (MPCs) through a two-phase synthesis method [16]. It has been identified that about 60% of the metal cluster surface is covered, whereas the coverage is only 30% on two-dimensional (2D)-surfaces. MPCs are important in technology not only by giving a higher number density of molecules at the surface but also by preserving the nanodimension of the cluster. Being a soluble powdery nanomaterial, these clusters allow conventional techniques for their characterization.

While it is important to understand the structure of monolayers to predict as well as to modify their properties, a study of their phase transitions is important for any application utilizing molecular assembly. In fact the phase transition of monolayers as a function of temperature has become an important subject for investigation. Two-dimensional ordering of various kinds has been attractive from the perspective of fundamental science. The importance of structure and phase of SAMs in the surfactant, wetting, etc. properties shows the need to understand the phenomena in detail.

Ulman's book [10] and review [17] deal with the structure SAMs in detail. The application of various new techniques for the study of monolayers has resulted in an improved understanding of these systems. Poirier's review is a good source for scanning tunnelling microscopy (STM) characterization [18]. A recent review by Schreiber discusses the structure and growth of SAMs in general [19]. In view of all these, we shall restrict ourselves to the most recent studies. Wherever necessary, we shall provide the necessary background information.

Hostetler and Murray [20] and later Templeton *et al*. [21] reviewed the monolayer properties on gold cluster surfaces. However, a structural perspective on alkanethiol monolayers on 2D and three-dimensional (3D) surfaces and an appropriate comparison between the two are lacking in the literature. This comparison is necessary to extend the characteristics of monolayers from planar to cluster surfaces. Even though the importance of phase transitions of monolayers has been recognized, an overall view of the temperature dependence of monolayer properties is not available.

Here, recent developments in the characterization and phase transitions of 2D and 3D monolayers will be discussed and compared. We may have to touch on some earlier research so that there is continuity in the presentation. We focus on alkanethiol monolayers on Au and Ag surfaces, giving more emphasis to the former. We believe this will help the reader to have a wider perspective on the properties of monolayers and their temperature dependence and will help to fabricate thermodynamically stable monolayers with an understanding of their temperature-dependent 2D phase behaviour. As a consequence of the above-mentioned objective, the literature cited is not exhaustive. Certain aspects not concerning the subject matter at hand, such as studies using SAMs as model surfaces, applications, etc., have been omitted completely. We offer our sincere apologies to those whose important work is not cited. We must caution the reader that some of the terminologies used here such as order and melting are rather loose; they imply limited translational periodicity and a phase transition from nearly solid to liquid-like phase respectively.

2. SAMs on planar (2D) surfaces (2D-SAMs)

2.1. *Preparation*

Most of the alkanethiolate SAMs have been prepared on the Au (111) face, which can be obtained by evaporating Au on polished glass slides. Even though several different solvents can be used at low thiol concentrations (mM), absolute alcohol is the most commonly used solvent. A schematic of the various steps involved in the formation of SAMs is shown in figure 1. The substrate Au is immersed into an ethanolic solution of the desired thiol. Even though thiols adsorb very rapidly on the surface, it is necessary to use adsorption times of the order of 12–15 h to obtain well-ordered, defect-free SAMs [10]. The driving force for the spontaneous formation of the 2D assembly includes the chemical bond formation of the adsorbate with the surface and the strong intermolecular interactions. The structure of the monolayer depends on the adjacent environment (solvent) as shown by Anderson *et al*. [22]. Studies suggest that annealing of the gold substrate gives defect-free SAMs [23]. Alkanethiol monolayers have been prepared also by the dissociative chemisorption of disulphides. Asymmetric disulphides ($R_{(n)}S–SR_{(n-m)}$) show a deviation from the 1:1 composition ($R_{(n)}S:SR_{(n-m)}$) with a predominance of longer chains ($R_{(n)}S$) [24]. This may be due to the increase in interchain van der Waals interaction in long-chain thiols. SAMs on Ag (111) surfaces are also prepared using the same procedure [10].

2.2. *Characterization*

Studies on various properties of monolayers have been grouped under different techniques. Several of these studies have used more than one technique and repeated references to them may be found.

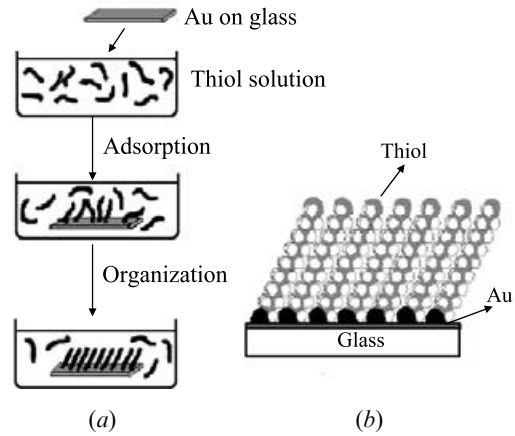

Figure 1. (*a*) Schematic of the various processes involved in the preparation of SAMs. The substrate, Au on glass surface, is immersed into an ethanolic solution of the desired thiol(s). Initial adsorption is fast and then an organization follows which should be allowed to continue for >15 h for the formation of a densely packed monolayer. (*b*) Schematic of a fully assembled SAM using a space-filling model of the thiol molecule. [Adapted from a figure available at http://www.ifm.liu.se/Applphys/ftir/sams.html]

2.2.1. *Ellipsometry*

Information on the thickness of monolayers is obtained from ellipsometric measurements. The technique measures the ellipsometric angles ψ and Δ (relative phase shift Δ and amplitude ratio ψ between the s- and p-polarized components of the probing laser) and are related to the optical properties and composition of the substrate and overlayers, by their thickness and morphology. Comparison of Δ and ψ for the monolayer-covered and uncovered surfaces allows the calculation of the thickness of the film [10]. Porter *et al.* [25] measured the thickness of a homologous series of monolayers $CH_3(CH_2)_nSH$ where $n = 1, 3, 5, 7, 9, 11$ and 21 and studied the dependence of n on the thickness of the monolayer. For alkyl chains with $n \leq 7$, a lower thickness than expected from the long-chain thickness has been measured. This is attributed to the lower packing densities that lead to a lower refractive index and thereby a lower measured thickness. The ellipsometric data suggest that the structure of the short-chain *n*-alkanethiol assemblies is more disordered than that of the long-chain ($n \geq 9$) assemblies. Thus, in addition to the measure of thickness, ellipsometric data give the effect of chain length on the order of the monolayer. One of the drawbacks of ellipsometry is that the optical constants of the gold surface and self-assembled monolayers must be known for the thickness measurement. One can circumvent this by using the infrared spectroscopic ellipsometry (IRSE) technique, which measures the changes in the polarization of the electric field vector. Recently, Meuse used IRSE to study the composition and molecular structure of the self-assembled monolayers of alkanethiols on gold surfaces [26]. This technique helps to obtain the structure, composition, thickness and morphology in the same measurement at the same sampling area. Optical frequency ellipsometric spectra showed the presence of a 1.2 ± 0.4 Å thick S/Au interface layer [27]. The presence of two optical transitions exhibited by this layer indicates a perturbation of the near-surface gold electronic structure on thiol adsorption.

2.2.2. *Surface plasmon resonance (SPR)*

SPR is used for the *in situ* study of the formation of SAMs. This technique is based on the angle-dependent reflection of a p-polarized laser beam. At a particular angle of incidence, called the 'SPR angle' (where total internal reflection occurs), the laser light excites the surface plasmons (collective oscillation of surface electrons) into resonance and an evanescent field forms on either side of the metal. At this point, reflectance from the surface will be at a minimum. This angle strongly depends on the refractive index of the medium over the surface of the metal and the thickness of the overlayer [28]. The SPR spectra of a gold film before and after the film formation show a shift in the plasmon resonance to larger angles due to the film formation. The thickness of the film can be calculated by comparing the data and assuming the dielectric constant of the chain. Chechik *et al.* studied the surface coverage, order and chain orientation of the SAMs of branched thiols and disulphides using Fourier transform infrared (FTIR), atomic force microscopy (AFM) and SPR [29] methods. Their SPR studies reveal that the monolayers formed by the disulphides were significantly thinner than SAMs of the thiol counterpart. This is explained as due to the lower coverage of the Au surface in SAMs of disulphides. They have used FTIR spectroscopy to confirm this observation. Exchange kinetics of octadecanethiol SAMs by octanethiol SAMs were studied using an *in situ* measurement of the reflectivity in the attenuated total reflection geometry with SPR enhancement [30]. This revealed a variation in exchange kinetics with exposure times of octanethiol solution, those exposed for longer having a high rate of exchange. This has been explained as due to the formation of dimers during the long exposure time, which adsorb less strongly than the monomer. Peterlinz and Georgiadis have measured the film thickness and film dielectric constant using two-colour SPR experiments [31]. They have shown that at least three kinetic steps are involved in the film formation; the first and third are the most rapid and the slowest and can be fitted with the Langmuir adsorption model. The kinetics of the second step is of zeroth order and depends on alkanethiol chain length, concentration and partial film thickness. Nelson *et al.* demonstrated the application of near-infrared SPR measurements for the accurate determination of film thickness and claimed that this is applicable even for a thicker film [32]. Ehler *et al.* reported an SPR study of alkanethiol monolayers on Au and Ag surfaces [33]. They have shown that the refractive indices for the alkanethiols increase on both Au and Ag surfaces with increase in chain length. Further, they have shown that the tilt angle of alkanethiol monolayers on Ag begins to increase from 0° starting with $n = 15$; however, on Au, an average tilt angle of 41° is reported and is independent of chain length [33]. One important application of SPR studies is in understanding biomolecular interactions using SAMs as templates [34, 35].

2.2.3. *Second harmonic generation (SHG)*

The linear dependence of the second harmonic signal on the adsorbate–substrate interaction allows *in situ* measurement of the monolayer coverage on the surface. The SHG process is sensitive to many aspects of the molecules at surfaces including concentration, orientation, chirality, oxidation state and electronic properties. An SHG study by Dannenberger *et al.* explains the kinetic model for the monolayer formation [36]. Their study showed that, in different solvents and at different concentrations, only Langmuir adsorption kinetics could explain the data. They proposed a model in which the displacement of the adsorbed solvent by the thiolate

becomes the rate-limiting step. Buck *et al*. showed that the average thiol coverage is constant for thiols longer than hexanethiol [37]. A coupled SHG, SPR and AC impedance study was performed by Zhang *et al*. [38]. They have shown that a linear relationship exists between the film coverage and second harmonic signal with increase in second harmonic response with decreasing coverage. The weaker potential dependence of the second harmonic signal from the metal/SAM/electrolyte system than from the bare Au or Ag surfaces is explained in terms of a series capacitor model for the SAM–double layer combination. Surface coverage and molecular orientation in polar SAMs have been studied using SHG [39]. The orientation was found to be $32^\circ \pm 3^\circ$, and surface coverage was $\sim$2–4 molecules nm^{-2}.

2.2.4. *X-ray photoelectron spectroscopy (XPS)*

XPS has been used to estimate the thickness, coverage, order and tilt angle as well as the orientational order. It is possible to calculate the thickness of the monolayer as explained by Beard and Brizzolara [40]. This is based on the area ratio of the C 1s photoelectron and carbon (KVV) Auger peak. Using an angle-dependent measurement, we have shown that the order of the monolayer is at a maximum when n is around 8 [41]. Moreover, the growth kinetics of SAMs have been monitored with XPS and it has been found that the rate of adsorption of short-chain thiols is higher than that of longer ones [42]. Using high-resolution XPS, Ishida *et al*. studied the nature of Au–S binding properties [43]. They have shown an orientational change of the Octadecanethiol (ODT) molecule after annealing, from a tilted to a near-parallel orientation. However, this kind of behaviour has not been detected by any other technique. The tilt angle of dodecanethiol monolayer on Au (111) has been calculated to be 30° using angle-resolved XPS, which is based on a photoelectron forward-scattering analysis [44]. This value is in good agreement with other literature reports. Heister *et al*. used synchrotron-based high-resolution XPS [45]. From the full width at half-maximum (FWHM) of the core photoemission line, they drew conclusions about the heterogeneous adsorption sites on both Au and Ag surfaces. Himmelhaus *et al*. studied the adsorption kinetics of docosanethiolate monolayers on the Ag (111) surface using XPS and near-edge X-ray absorption fine structure [46]. They demonstrated a domain growth mechanism, where alkanethiolate molecules nucleate around the initial alkanethiolate islands. The presence of two sulphur species on Au and Ag surfaces has been suggested using high-resolution photoelectron spectroscopy [47]. The two sulphur species possess chemical and geometrical inequivalence as indicated by the 1.3 eV difference in binding energy and intensity variations. The intensity of the two sulphur species strongly depends on the take-off angle. The observed effects are suggested to be due to X-ray photoelectron diffraction. The different photoelectron diffraction observed for the S 2p photoelectrons of the two species reveals that either the two atoms are at different heights with respect to the surface plane or the alkyl chain conformation is strongly different for the two species, assuming the scatterer is S and C respectively.

2.2.5. *Wettability*

These measurements directly reflect the structure and composition of the surface. In this method, the contact angle (θ_{eq}) formed by a droplet of a probe liquid on a monolayer-coated surface is measured: this is related to the surface free energies (γ) by the equation $\gamma_{sv} = \gamma_{sl} + \gamma_{lv}\cos(\theta_{eq})$ at thermodynamic equilibrium, where the subscripts s, l and v refer to substrate, liquid and vapour respectively. The practical

inability to attain equilibrium during the measurement causes a hysteresis in the contact angle. The advancing (θ_a) and the receding (θ_r) contact angles represent the metastable equilibrium states of the probing liquid on low- and high-energy regions of a surface respectively. The hysteresis between θ_a and θ_r provides a measure of the degree of surface roughness or heterogeneity of the interface [10]. Miller and Abbot explained the increased wettability in the case of shorter-chain alkanethiolates compared with the longer ones [48]. This is because, in shorter-chain monolayers, the van der Waals interactions between the contacting liquid above the monolayer and the underlying gold substrate might be of sufficient strength to reduce the contact angle, thereby increasing the wettability. The influence of lateral van der Waals interaction within the SAMs also should be considered to explain this property. Hysteresis for well-ordered alkyl chain monolayers is around 10°, whereas it is around 30° in more disordered monolayers. Thus it serves as a measure for the order of the monolayer on the surface. Laibinis *et al.* compared the wetting properties of SAMs on Au and Ag [49]. They have shown that the structural difference on the two surfaces does not play a significant role in the wettability and the interfacial composition of SAMs is the primary factor determining the wetting properties.

2.2.6. *Thermal desorption spectroscopy (TDS)*

Various groups have studied the adsorbed states of thiols using TDS. In this method, the behaviour of thiol molecules on gold is studied during the desorption process [50]. Existence of dimer molecules on the surface has been reported by Mohri *et al.* [51] which is in agreement with the SPR studies of Kajikawa *et al.* [30]. Using a comprehensive TDS study, Noh *et al.* [52] explained the existence of different adsorption sites and showed that dimerization plays a major role in SAM formation and desorption. Kondoh *et al.* examined the surface coverage dependent desorption process of SAMs using STM and TDS [53]. They explained that alkane thiolates in the denser phase (more coverage) desorb as disulphides, whereas the low-density phase desorbs in the form of thiolate radicals. These changes have been explained in terms of molecule–substrate bonding.

2.2.7. *Microscopy and diffraction*

Electron diffraction studies show that the symmetry of the adsorbed sulphur atoms is hexagonal [54, 55]. The distance between the pinning sites is 5.0 Å and the available area for each molecule is 21.4 Å^2. This spacing is close to the spacing between the next nearest gold atoms on the Au (111) surface (4.9 Å). The chains show a tilt of 30° with respect to normal [56]. A detailed low-energy electron diffraction (LEED) study has been reported by Balzer *et al.*, where they explained the chain length dependence of the structure of SAMs on Au [57]. Helium diffraction studies suggested that the alkanethiols form a commensurate $(\sqrt{3} \times \sqrt{3})R30°$ overlayer [58]. Dubois *et al.* used LEED to compare the structure of alkanethiol monolayers on Au (111) and Au (100). They have reconfirmed the $(\sqrt{3} \times \sqrt{3})R30°$ structure on Au (111) while a $c(2 \times 2)$ structure is observed on Au (100) [56].

AFM and STM are two powerful tools for the characterization of surfaces with atomic-scale resolution [59]. STM images are obtained as a result of electron tunnelling between the tip and the surface and AFM maps the force acting between the tip and the surface. After the invention of AFM, a variety of scanning force microscopy (SFM) techniques have been developed which detect electrostatic,

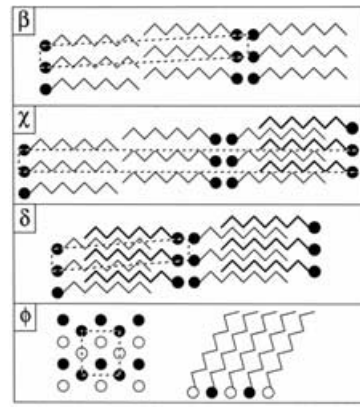

Figure 2. The phases were described as α, β, χ, δ, ε and ϕ, where α is a two-dimensional gas with a low density, and highly mobile molecules, β, χ and δ are stripped phases with molecular packing areas of 82.8, 64.8 and 54.0 Å^2/molecule respectively, and ε and ϕ phases are the two-dimensional liquid and the upright phases respectively. (From Poirier [66].)

frictional or magnetic forces between the SFM probe and the substrate. In chemical force microscopy, it is possible to obtain valuable information on the chemical specification at the surface using a chemically modified probe tip [60].

STM studies show that the gold–alkanethiolate SAMs have a hexagonal $(\sqrt{3} \times \sqrt{3})\,\text{R}30^\circ$ structure in which sulphur atoms occupy the 3-fold hollow sites of the Au (111) surface with a lattice constant of 5 Å [61]. The adsorption and desorption processes of hexanethiol SAMs on Au (111) were studied with STM [62]. Studies showed the presence of an additional $c(4 \times 2)$ superlattice structure of the SAMs, and this is attributed to the different adsorption states of thiols such as thiol monomer and dimer. A $c(4 \times 2)$ superlattice structure has been observed after long exposures. Strong and Whitesides showed that the bonding of the sulphur in alkanethiol is more complicated on Au (100) than on Au (111); in the former a densely packed $c(10 \times 10)$ overlayer is formed [54]. An STM study by Poirier reveals a distorted hexagonal arrangement with $c(2 \times 8)$ unit cell structure for butanethiol SAMs on Au (001) [63]. Schweizer *et al*. showed the absence of vacancy islands on the Au (100) surface on thiol adsorption [64]. *In situ* STM helps in studies of the dynamics of SAMs on the surface [65]. Using ultrahigh vacuum (UHV) STM, Poirier revealed the coverage-dependent phases and phase stability of SAMs [66]. It has been shown that the monolayer adopts six discrete structural phases with increase in coverage. At low coverage, alkanethiol exists as a lattice gas, which changes to islands of a commensurate crystalline lattice that grow in equilibrium with the lattice gas until saturation; finally, above saturation coverage of the densest surface, an aligned phase results. These phases are shown in figure 2. Their temperature behaviour will be discussed in the next section. Heinz and Rabe used STM to study the chemisorption of alkanethiolates on Ag (111) and have shown that they form a hexagonal lattice [67]. These thiolates form a $(\sqrt{7} \times \sqrt{7})\,\text{R}10.9^\circ$ structure on Ag (111) surfaces. Thorough STM investigations of SAMs have been carried out, and the results have been reviewed by Poirier [18].

An AFM study of alkanethiol monolayers revealed their arrangement on gold surfaces [68]. The images show a periodic hexagonal pattern of equivalent spacings

with nearest-neighbour distance of 0.52 ± 0.03 nm and next-nearest-neighbour distance of 0.90 ± 0.04 nm [69, 70]. This agrees with the $(\sqrt{3} \times \sqrt{3})$ R30° structure reported by Alves and Porter [71]. Tamada *et al.* [72] observed that the film coverage increased with the immersion time, and a totally covered surface was observed after 3 min of exposure. *In situ* AFM studies of the desorption of monolayers revealed that the molecules detach from the hole–monolayer boundaries and remain adsorbed in the hole regions at a very low concentration and from there they eventually desorb into the solvent [73]. This is essentially the reverse phenomenon observed for monolayer growth.

A grazing angle X-ray diffraction study by Fenter *et al.* confirms the $(\sqrt{3} \times \sqrt{3})$ R30° structure [74]. They found that the monolayer has a domain size of ~90 Å (as deposited), while the annealed (at 363 K) one has a domain size of 1000 Å, comparable with the substrate domain size. This experiment shows that defects play an important role in the structure of the as-deposited monolayer. They have shown that the top-layer Au atoms are laterally relaxed away from the their bulk lattice and explained the effect of chain length on the tilt structure of the monolayer. A lattice constant of 4.6–4.7 Å is observed for octadecanethiol monolayers on Ag (111) surfaces [75].

2.2.8. *Electrochemical studies*

Electrochemical techniques such as cyclic voltammetry (CV) and impedance spectroscopy are widely used for SAM studies [76]. Electrochemistry is a useful technique to see the defects in the monolayer. The two kinetics steps in SAM formation and the presence of pin-hole defect free SAMs have been shown by CV studies [77]. Oxidative desorption of short-chain alkanethiols is observed at 1.15 V [78]. Mohtat *et al.* used CV to study the behaviour of alkanethiols on Ag surfaces [79]. They observed two current peaks in the CV curves which are attributed to the two-step reduction of alkanethiols. They further used chronoamperometric measurements to support the two-step reductive desorption of alkanethiols. Boubour and Lennox have shown that SAMs on Au surfaces act as an ionic insulator up to a critical cathodic potential, and, at higher cathodic potential, they allow ion penetration and this critical potential is a function of chain length of the alkane moiety [80]. Hatchett *et al.* measured the free energy of adsorption of *n*-alkanethiolates at Ag (111) surfaces using CV [81]. The two voltammetric curves during adsorption are attributed to the two distinct steps in the formation. The low-coverage phase is independent of alkane chain length and the energetics of adsorption is determined by the strength of the Ag–S bond, whereas the other at full monolayer coverage is a function of the alkane chain length where the hydrophobic interactions and intermolecular forces between the alkyl chains dominate. The free energies of adsorption at these two phases have been calculated as $\Delta G = -22.8\,\text{kcal mol}^{-1}$ and $\Delta G = -16.6\text{–}1.02n_c\,\text{kcal mol}^{-1}$ respectively, where n_c is the number of carbon atoms.

2.3. *Vibrational spectroscopy*

2.3.1. *IR spectroscopy*

All-*trans* behaviour of alkyl chains has been confirmed by FTIR studies [82]. IR spectroscopy is a powerful tool for the characterization of SAMs taking advantage of the sensitivity of the vibrational modes to the environment. The spectra of SAMs

are usually obtained in the reflection absorption mode, where the incident light is reflected at an angle of 80° (relative to surface normal) to maximize the absorbance by the monolayer [83]. Surface selection rules in IR allow only transition dipoles with a component perpendicular to the surface to be observed. Thus this technique gives information on the structural orientation in addition to the order. IR studies suggest that the monolayers will be well ordered when the number of carbon atoms is around eight. Short-chain alkyl thiols show a 2-D liquid phase at room temperature. This liquid phase has been observed in STM measurements also [84]. The symmetric and asymmetric C–H stretching modes of methyl (r^+ and r^-) and methylene (d^+ and d^-) groups are indicative of the crystallinity of the sample [85]. In the case of alkanethiol monolayers on a gold surface, the values for the d^+ and d^- modes (2850 cm^{-1} and 2920 cm^{-1} respectively) correspond to those of the crystalline alkanes when n is more than 8. This indicates higher order in longer-chain alkanethiols. Methyl modes (r^+ at 2877 cm^{-1}, r^- at 2963 cm^{-1}) suggest that orientational freedom exists on the chain termini. It is possible to calculate the tilt angle of the alkyl chain from the d^+ and d^- modes, and it has been shown that alkyl chains tilt around 30° with respect to the surface normal. It is shown that irrespective of (100) or (111) surface, alkanethiol films form ordered monolayers on Au [56]. Using FTIR external reflection spectroscopy, Terrill *et al*. have shown that the crystallinity of SAMs increases with the immersion time and concentration and becomes a constant in the 10^{-6}–10^{-2} mM concentration range [86]. Laibinis *et al*. used reflection IR spectroscopy for the characterization of alkanethiol monolayers on coinage metals [83]. They have shown that alkanethiols form an all-*trans* zigzag arrangement on the Ag (111) surface as in the case of Au (111). The difference lies in the tilt angle from the surface. They calculated the tilt angle of the alkanethiols on Ag (111) as 12° and the twist angle to be 45° [83].

Because of the low sensitivity as a consequence of the low number density of the molecules on the surface, enhancement of the signal is essential for the proper detection of monolayers. In surface-enhanced IR reflection absorption spectroscopy, an enhanced signal has been used to gain detailed structural information [87–89].

2.3.2. *Raman scattering*

As a result of the rather stringent selection rules of surface Raman scattering [90], it can reveal important structural information. Surface-enhanced Raman spectroscopy (SERS) in spite of being surface sensitive can be applied only to rough surfaces [91]. Bryant and Pemberton used SERS for the study of alkanethiols on gold [92]. The study suggested an increased order for long-chain alkanethiol monolayers. We have studied alkanethiol monolayers on polycrystalline gold films [93] and have shown that order of the monolayer is chain length dependent. We observed the kinetic steps in the formation of SAMs, the initial adsorption followed by a slow self-assembly. In both lower and higher homologues, the initial exposure leads to the preferential formation of the *gauche* form and the *trans* form begins to gain in intensity quickly. Bryant and Pemberton carried out a comprehensive study on the structure of alkanethiol monolayers on silver surfaces using SERS. They have shown that longer-chain monolayers are highly ordered as in the case of gold surfaces [94]. Lee *et al*. showed the presence of two distinct CS stretching bands of alkanethiolates on the Ag surface, one being favourable at submonolayer coverage and the other at full coverage [95]. These two bands are attributed to the multiple adsorption sites of

the thiolate such as the bridge site or the four-fold site and the on-top site respectively.

2.3.3. *Sum frequency spectroscopy (SFS)*

SFS is non-linear vibrational spectroscopy where the second-order non-linear optical process involved makes it forbidden in isotropic and centrosymmetric media. Since the adsorbed molecules do not possess a centre of symmetry, SFS can provide information about the structure, molecular conformations and orientations on the surface [96]. In SFS two pulsed laser beams at frequencies ω_1 and ω_2 are overlapped at the interface. Frequency ω_1 is usually fixed in the visible region whereas ω_2 is tunable in the IR region. Light emitted from the surface will be detected and this will be the sum of ω_1 and ω_2. The intensity of the emitted light is resonantly enhanced when ω_2 matches with the molecular vibration of the adsorbed molecules. The technical aspects of the IR–visible sum frequency generation (SFG) have been reviewed by Himmelahaus and Buck [97]. Himmelhaus *et al.* used SFS to study the kinetics of alkanethiol SAM formation [98]. They concluded that a three-step kinetics existed: the initial adsorption, slow self-assembly and reorientation of the terminal methyl group. The high sensitivity of SFS allowed them to distinguish the third step. Biphenyl methylene thiol SAMs on gold and silver surfaces has been studied and it has been shown that the gold substrate shows a non-resonant contribution as a function of visible beam wavelength [99]. An SFS study of the solvation of oligo(ethylene glycol) terminated monolayers revealed that the film structure is strongly disturbed by the interaction of liquid with the monolayer [100]. This disordering of monolayers in the presence of a liquid is also reported by another group where they used a poly(ethylene glycol) terminated monolayer [101].

2.4. *Structure of SAMs: an overall view*

Ab initio calculations confirm the $(\sqrt{3} \times \sqrt{3})$ R30° structure for alkanethiolate SAMs on the Au (111) surface [102]. There are two chemisorption modes present for the thiolates at Au (111) surfaces, one with an Au–S–C bond angle of 180° (sp hybridization), and another with ~104° (sp^3 hybridization). They found that both these are closer in energy and these structures may be present on each domain. Why the surface atom prefers the hollow sites rather than the on-top site or bridging site is an interesting question. Through their calculations Sellers *et al.* [102] suggest this to be because of the combination of both electrostatic effects as well as lateral discrimination. Sulphur atoms bound to the on-top-sites have a net charge of *ca.* $-0.7e$, whereas in the hollow sites it is *ca.* $-0.4e$. All-*trans* alkyl chains with a tilt angle of 30° have been proposed. Gronbeck *et al.* used density functional theory to obtain the structure, binding energies and the type of bonding present in SAMs of alkanethiol and disulphides on Au surfaces [103]. They showed that disulphides undergo dissociative adsorption and thiols adsorb with the loss of thiolate proton in the form of molecular hydrogen.

Sulphur atoms bond to the three-fold hollow sites on the Au surface and the extremely strong surface bond (44 kcal mol^{-1}) contributes to the stability of the SAMs. Several studies exist on the adsorption energetics of SAMs, but all are not completely consistent [104–106]. Electron diffraction and STM measurements reveal that the monolayers form a $(\sqrt{3} \times \sqrt{3})$ R30° overlayer structure, which is a balance between the S–Au chemisorption and the interaction between the chains. Zarnikov *et al.* demonstrated that the hybridization and thus the spatial orientation of the

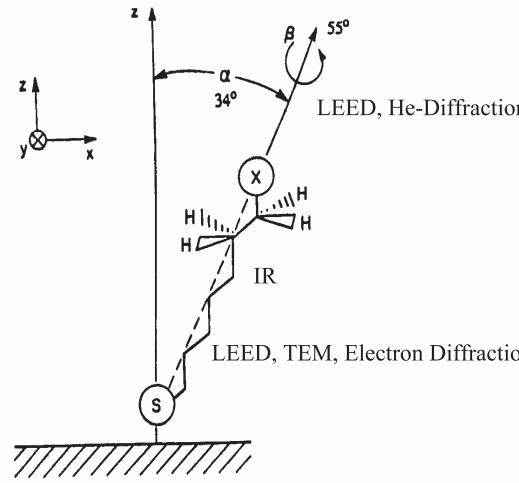

Figure 3. All-*trans* arrangement of alkanethiol monolayer on Au (111) surface. The tilt and twist angles are shown. (From Dubois and Nuzzo [211].)

bonding orbitals of sulphur is the determining factor for the orientation and density of the alkanethiol monolayer rather than the intramolecular interaction [107]. The surface order can extend over hundreds of square nanometres and the symmetry of the sulphur atoms is hexagonal. The distance between the pinning sites is 4.99 Å, which is nearly three times the van der Waals diameter of the sulphur atom (1.85 Å). Thus sulphur–sulphur interactions are believed to be minimal. This distance is greater than the distance of closest approach of the alkyl chains (4.24 Å), which makes the monolayer tilt. This tilt angle (α) is found to be 30° with respect to the surface normal towards the nearest-neighbour direction. Fenter *et al.* demonstrated a systematic dependence of the tilt structure (tilt angle and tilt direction) on the chain length, explained as being due to the change in intralayer interaction strength [108]. The twist angle β (defines the rotation of the alkyl carbon backbone about the chain axis with respect to the plane defined by the chain axis and the surface normal) for the long-chain alkanethiol is found to be ~52°, which implies that Au–S–C bond angle is nearly 120°, close to the optimum value for the sp^2-hybridized sulphur atoms. A schematic side view of a monolayer chain on an Au surface is presented in figure 3.

2.4.1. *Initial stages of adsorption*

Extensive XPS experiments suggest that chemisorption of alkanethiols on a gold (0) surface yields the gold (1) thiolate ($R–S^-$) species, although the mechanism is not clear. The presumed adsorption chemistry is $R–SH + Au_n^0 \rightarrow RS^-–Au^+ + (1/2)H_2 + Au_{n-1}^0$. The absence of S–H stretching in the IR spectrum suggests the loss of hydrogen from the thiol. This loss might happen via the reductive elimination reaction of the gold(II) hydride (formed by the oxidative addition of the alkanethiol) or by the elimination of hydrogen as shown above or as water in the presence of an oxidant. However, using electrochemical measurements, Eu and Paik showed that it is not just a simple mechanism, but an electrochemical oxidation route is involved [109]. The formation of alkanethiol SAMs is suggested to involve an anodic reaction, $RSH + Au \rightarrow RS–Au + H^+ + e^-$.

We have seen hydrogen evolution during monolayer formation [110]. For this experiment large area gold/silver mirrors were prepared and the mass spectrum of the gases was monitored during thiol adsorption. Experiments were also done with citrate-stabilized gold colloid in water and the citrate cover was exchanged with alkane and aromatic thiols.

2.4.2. *Growth processes*

The growth kinetics of SAMs have been studied using different techniques and it has been shown that growth follows first-order Langmuir adsorption kinetics, $d\theta/dt = -k(1-\theta)$, where θ is the fraction of occupied sites, t is the time and k is the rate constant which contains the effects of the flux of thiol molecules to the surface and the sticking coeficient [111]. The sticking probability (the probability of adsorption per molecular collision with the surface) of alkanethiols is found to be increasing from 10^{-8} to 10^{-6} as the alkyl chain length increases from 3 to 19 carbon atoms. The transition state of adsorption is stabilized by $\sim 0.7\,\mathrm{kJ\,mol^{-1}}$ per CH_2 group [112]. Biebuyck *et al*. performed a detailed study of the kinetics of formation of these SAMs [113]. All kinetic studies suggest fast adsorption followed by slow self-assembly. By measuring the coverage, energetics and structure as a function of growth rate and temperature, Schreiber *et al*. gave a quantitative description of the molecular processes involved in the self-assembly process [114]. For this they used vapour-deposited films. They explained that the detailed growth behaviour would depend on variables such as solvent (with or without solvent), molecular rigidity and the surface–head group chemistry. The adsorption kinetics of decanethiol monolayer vapour deposited on the Au surface has been studied using grazing angle incidence [115]. This shows two distinct adsorption mechanisms. One is linear and the second involves an associative mechanism in which the growth rate increases quadratically with the molecular impingement rate.

During the first step of film growth, some molecules adsorb independently and act as nucleation centres for domain growth. Thus, in each domain, each monolayer has the same sulphur adlattice and the same tilt direction. This resulted in the formation of domain boundaries and a domain-like growth of the SAM. STM measurements reveal the existence of hexagonal patterns as well as several variants of $c(4 \times 2)$ superlattices [116]. This study further showed that the domain boundaries are oriented along the next-nearest-neighbour directions of the sulphur lattice. Various studies suggest that the polymethylene chains are fully extended, tilted with respect to the surface normal, and are in nearly all-*trans* configuration. With increasing chain length of the adsorbed thiol, the thickness increases linearly. For shorter chain length, a liquid-like behaviour is observed at room temperature. This is because of the decreased van der Waals interaction in the short-chain thiols. It has been shown that vacancy islands (holes) are being generated during the self-assembly process [117] and this can be healed out by thermal annealing at 350 K [118].

It is known that the silver surface is more highly susceptible to oxidation than gold. In most of cases, silver forms an oxide layer prior to SAM formation and the silver oxide layer reacts with the adsorbate. Thus the chemistry during adsorption may be different to that on gold. The absence of silver oxide in SAMs indicates that the oxide must be replaced by thiols or it undergoes reduction. Because of its susceptibility to oxidation, special care has to taken with the preparation of monolayers.

2.4.3. *Structure of monolayers on silver*

Alkanethiols on Ag (111) form a $(\sqrt{7} \times \sqrt{7})$ R10.9° structure with an S–S distance of 4.41 Å. Because of this shorter S–S distance, alkanethiols on Ag are more densely packed. As a result of the difference in the amount of oxides present on the surface, different reports exist on the tilt of the alkyl chains on Ag (111) surfaces; however, the orientation has been proved to be almost perpendicular to the surface on clean Ag (111) surfaces [119]. It has been shown that the $(\sqrt{7} \times \sqrt{7})$ R10.9° structure observed in the short-chain alkanethiols cannot be extended to the long-chain alkanethiolates because of the larger interchain van der Waals interaction [17]. The suggested mechanism for the formation of alkanethiolate SAMs on the Ag (111) surface is the initial formation of the $(\sqrt{7} \times \sqrt{7})$ R10.9° structure and its distortion on saturation coverage due to the increase in van der Waals interaction. The packing observed in alkanethiols on the Ag (111) surface is close to the effective packing of the alkyl chain. This results in the near-perpendicular orientation of molecules on the surface. In the case of Au (111), the alkyl chain is tilted 30° from the surface normal to decrease the lattice energy. The difference in orientation is mainly due to the interchain van der Waals interaction. A recent review by Zharnikov and Grunze explains the difference and similarity of the behaviour of alkanethiols on Au and Ag surfaces [120]. They demonstrated that the decisive factor for the structure and bonding in these systems is the head group–substrate interaction. Using different spectroscopic studies of alkanethiols, fluorocarbon thiols and aromatic thiols, they showed that a significant driving force exists to enable sp^3 and sp hybridization of sulphur head groups on gold and silver surfaces respectively.

2.5. *Stability of the monolayer*

It is shown that alkanethiol SAMs are stable in air at room temperature, whereas they undergo oxidation in presence of ozone as revealed by Schoenfisch and Pemberton [121]. Zhang *et al.* have shown that ultraviolet (UV) irradiation also results in the formation of sulphonates on the surface, the oxidation product of the sulphur end of the thiol [122]. The extent of oxidation is dependent on the alkane chain length, the shorter-chain alkanethiols being oxidized more rapidly. This is because diffusion of ozone is slower in the longer-chain thiols than in the shorter-chain thiols.

Calculations defining the optimum structure of SAMs show that the molecules begin to rotate and the *gauche* defects increase as temperature increases. In the next section we will review the phase transitions of 2D monolayers as a function of temperature.

2.6. *Phase transitions*

Conformational transitions play a major role in the temperature-dependent phase behaviour and dynamics of molecular thin films. The importance of such distinct phases in the surfactancy, wetting, etc. properties shows the need to understand the microscopic characteristics of such phenomena in detail [123]. Only a limited number of studies have addressed the issue of phase transitions of alkanethiol monolayers on Au surfaces. Recent investigations have shown that heating induces changes in the vibrational, conformational and positional order parameters. These studies show that vibrational spectroscopic measurements are sensitive to the conformational order, and on the other hand diffraction and scanning probe measurements are sensitive to the spatial position of the molecule.

We shall look through some of the most prominent studies dealing with the phase transitions in the following sections. Each of these has been grouped under the technique used.

2.6.1. *Helium diffraction*

During low-energy helium diffraction experiments with alkyl thiol monolayers on gold, Chidsey *et al.* [124] found that the diffraction peaks gradually lose intensity as the surface temperature is raised and they disappear around 100 K; the specular peak itself disappears at 300 K. They attributed this to the thermal motion of the CH_3 group located at the surface. This has been further confirmed by Camillone *et al.* [125] who suggested an increase in thermal motion with increase in temperature. This finding is consistent with the experiment by Nuzzo *et al.* [126] who used IR spectroscopy to show that alkyl chains undergo a phase transition, below 300 K, from an ordered phase to another ordered phase, where the transition temperature is chain length dependent.

2.6.2. *Molecular dynamics (MD)*

MD simulations suggest a sudden increase in rotational disorder at 200 K along with the onset of conformational disorder as temperature increases [127]. Direct experimental evidence for such a transition is still lacking; however, IR data show a two-sublattice low-temperature structure below 220 K. This simulation suggests a correlation between the rotator phase transition and the appearance of the conformations arising indirectly via the softening of torsional potential and enhanced flexibility of the chain backbone. As the temperature increases, a second transition occurs, the unlocking of the direction of tilting between 250 and 300 K. The tilt direction is locked in the nearest-neighbour direction below 250 K and fluctuates between nearest-neighbour and next-nearest-neighbour directions above 300 K. The tilt angle of the chains continues to decrease with temperature until, above $T \sim 450$ K, the system no longer has a collective tilt. At this temperature, the molecules are freely rotating and have a high density of conformational disorder, and they are distributed uniformly throughout the chain. An MD study by Mar and Klein [128] using an all-atom model re-established the rotator phase and the high-temperature phase transition. This study shows a herringbone structure (two chains per unit cell) at low temperature, which is contradictory to the experimental observation of the four chains per unit cell structure. Hautman *et al.* suggested large amplitude librations and rotational jumps about the molecular axis at 300 K, rather than free rotation [129], through their MD simulations. Using a Monte Carlo technique, Taut *et al.* [130] showed the 2D melting and a solid-state phase transition. Both of the low-temperature order–disorder transformations have been observed in an MD simulation by Bhatia and Garrison [131]. They proposed a mechanism for the higher-temperature melting transformation, which involves a gradual increase of 5–7 dislocation pairs and consequently non-six-fold coordinated atoms. This induces untilting and the introduction of a large number of *gauche* defects. Using Morse and Lennard-Jones potentials, Sadreev and Sukhinin calculated the P–T diagram of SAMs [132]. They claimed that three phase transitions are present in SAMs and all of them are first order.

2.6.3. *IR and Raman spectroscopy*

The nature of alkyl chain phase transitions has been investigated using IR spectroscopy. In IR, the degree of disorder is measured on the basis of the position

of the methylene-stretching mode and this is the most sensitive measurement of conformational disorder. IR investigations suggest that *gauche* conformations are concentrated at the chain termini and decreases with decreasing surface temperature [133]. Comparing the influence of temperature on the methyl and methylene modes, Dubois *et al*. [133] showed that the *gauche* defects are concentrated at the chain termini and, as the temperature is raised, the methyl group melts first and progresses towards the surface methylenes. Nuzzo *et al*. [126] observed that the monolayers are more ordered at 80 K. The conformation of the molecules is more all-*trans* and two alkyl chains per unit cell are observed. In these experiments, a peak assigned to the methylene group asymmetric scissoring motion is observed to split into two as the temperature is lowered from room temperature. However, IR evidence for the orientational phase transition has not been observed in low-temperature diffraction experiments.

Reflection absorption IR spectroscopy (RAIRS) investigations at near-grazing incidence show a phase transition from a crystalline state to a liquid-like state at around 350 K [134]. The upward shift of peak frequency and decrease in intensity as well as increase in the peak width are indications of this phase transition. This solid–liquid phase transition is gradual and irreversible, unlike in lipid bilayers. The coexistence of both the liquid-like and the polycrystalline states in a wide temperature range is possible in these SAMs. The increase in frequency is attributed to the appearance of *gauche* conformational defects throughout the chain. Internal kink defects, which are stable conformations above 350 K, are present even when the sample is cooled down. The chain entanglement and strong interaction of the sulphur with the substrate prevent the quick return of the chain to its thermodynamically equilibrium state.

A two-step phase transition has been observed in RAIRS experiments on a series of alkanethiol SAMs [135]. A reversible structural change, that results from the untilting of the alkyl chain, is observed around 320 K, whereas a complete irreversible transition is observed above 350 K. This irreversible transition is due to the increase in the conformational disorder throughout the chain. Variation of the integrated intensity as a function of temperature is indicative of two phase transitions. An initial decrease in intensity is observed, followed by an increase around 350 K. The initial decrease is attributed to the change in the average tilt angle of the alkyl chain. Why the untilting occurs on heating is an interesting question. This can be explained as follows. Alkyl chains are tilted to increase the three-dimensional density of the monolayer. On heating, the vibrational motion must be accommodated by a decrease in the density of the alkyl chain. This happens through the untilting of the alkyl chain. Because of the surface selection rules of IR, RAIRS is the most sensitive tool to identify this change. Surface selection rules suggest that only vibrational modes whose components are perpendicular to the surface will be observed. Thus the variation of intensity in RAIRS can be explained as due to the variation in the tilt angle. This confirms the high sensitivity of IR to changes in the tilt angle. This variation is in accordance with the MD simulation for a C_{13} thiolate SAM, which suggests that the chains gradually untilt as the temperature is raised from 40 to 375 K, with the average tilt angle varying from 35° to 24° to the surface normal. The increase in intensity after 350 K is attributed to the formation of conformational disorder in the chains, leading to a random orientation of the methylene groups, which are perpendicular to the surface. In addition to the

integrated intensity, an upward shift of the frequency also occurs as a result of conformational disorder.

There are fewer phase transition studies of alkanethiols on Ag surfaces. Bensebaa *et al.* used silver alkanethiolate layered materials for the phase transition studies [136]. They have shown that the alkanethiols undergo a melting transition at higher temperature as in the case of Au SAMs. We have shown that octadecanethiolate layered materials show melting at 400 K, much higher than the phase transition temperature on the planar surface [137]. This is attributed to the increase in van der Waals interaction as a result of the interdigitation of the alkyl chain from the neighbouring layer. Voicu *et al.* used specifically deuterated silver octadecanethiolate layered material and studied its phase transition behaviour using differential scanning calorimetry (DSC), variable temperature IR and variable temperature nuclear magnetic resonance (NMR) spectroscopies [138]. They too found a melting transition at 403 K and attributed it to the increase in *gauche* population. Their study shows that the C_1 atom (closest to the substrate) experiences a more restricted motion. The phase behaviour of silver stearate was investigated by temperature-dependent diffuse reflectance IR Fourier transform spectroscopy [139]. Two step phase transitions were explained, the first one at 390–420 K, due to the formation of *gauche* conformers, and the second at 520–550 K, where decomposition of silver stearate leads to the formation of nanoparticles.

Raman spectroscopy is particularly useful in understanding the conformational order of the C–S mode. In our SERS investigations of SAMs, we observed the solid–liquid phase transition before desorption of the monolayer [93]. As the temperature increased, the intensity of all the peaks decreased; this is particularly visible in the $\nu(\text{C–C})_\text{T}$ and $\nu(\text{C–S})_\text{T}$ modes. We observed an increase in *gauche* conformations with temperature.

The SERS study of Teuscher *et al.* confirms the presence of two transitions [140]. An upward shift of the methylene stretching bands near 318 K indicates the increased conformational disorder and/or lateral movement of the alkanethiol. The absence of changes in the ν(C–C) and ν(C–S) bands suggests that this transition is only on the topmost portion of the monolayer. When the temperature is increased to 343 K, the *gauche* conformers closer to the surface begin to manifest. Moreover, the appearance of the 1080 cm^{-1} band, assigned to the $\nu(\text{C–C})_\text{G}$ vibration, shows an increase in the concentration of *gauche* conformers. This is attributed to the melt transition from the solid to the liquid-like behaviour. One important point they noticed here is that the melt phase of the SAMs is more ordered than the bulk thiol. This is attributed to the partial covalent character of the sulphur–gold bond, which constraints the sulphur only lateral motion, in turn limiting the conformational degrees of freedom of the alkane chains closer to the surface.

The MD simulations as well as IR studies confirm two phase transitions in the monolayers. The second phase transition has been proved by various experimental techniques. Fenter and coworkers performed a grazing-incidence X-ray diffraction study as a function of both chain length and temperature [74]. They showed different phases on the basis of tilt direction and constructed an (n, T) phase diagram. The phase transitions are dependent on chain length as well as temperature. As the temperature increased to 343 K, a melting transition is observed in long-chain thiols with the coexistence of both solid and liquid phase at temperatures in the range 323–343 K. This transition involves a change in the thiolate packing from a hexagonal,

two-dimensional structure that is commensurate with the Au (111) substrate to one that is incommensurate.

2.6.4. *Electrochemical and electrical properties*

Byloos *et al*. studied the temperature-dependent behaviour of the reductive desorption and oxidative adsorption of SAMs using CV [141]. They have shown that the two peaks present at low temperature merge into a single peak with increase in temperature during the reduction of the hexadecanethiol monolayer. Similarly, three peaks in the oxidation present at low temperature change to one peak at higher temperature. Using *in situ* vibrational spectroscopy they confirmed that this behaviour is due to phase transitions of the monolayer. The electrochemical studies carried out by Badia *et al*. confirm the order–disorder transitions in SAMs [142]. They too found a chain length dependence of melting temperature; the values vary between 313 and 338 K.

Recently AC impedance spectroscopy has been used to probe the temperature-dependent phase transition of the SAMs on a gold surface [143]. This technique involves the measurement of the frequency dispersion of the impedance or admittance of a system. It was observed that the activation resistance decreases above the phase transition temperature. This is attributed to the loss of order in the monolayer at higher temperature that results in an increase in permeability of the monolayer towards the redox probe and electrolyte and thereby decreases the resistance. It was further shown that the mass transport properties of the two phases are different, which supports the transition from an ordered impermeable phase to a disordered permeable phase. Recently the solid–liquid phase transition has been observed in an in-plane resistance measurement of the SAMs on a gold surface [144]. Here the observed increase in the slope of the resistance versus temperature plot is attributed to the phase transition.

2.6.5. *Contact angle*

In an earlier study Evans *et al*. found that the contact angle varies as a function of both chain length and temperature [145]. A fast increase in advancing contact angle is observed for the C_{11} monolayer at 298 K, and a gradual change followed by a sudden change at 323 K is observed for the C_{21} monolayer. This is attributed to the surface reorganization, which is the result of *trans–gauche* isomerization of the chain termini, and corresponds to the previous MD simulations as well as IR studies.

2.6.6. *Microscopy*

STM investigations suggest the existence of thermal motion for the alkyl thiol monolayers around 350 K, which in turn results in mobility for the topmost layer of the gold surface [146]. This mobility results in bigger holes or vacancy islands with triangular equilibrium shape. On extensive annealing at 350 K, the vacancy islands are annihilated at pre-existing substrate steps, leaving flat defect-free SAMs. The slow evaporation rate compared with the lateral mobility of the molecule allows the film to adopt new stable structures for each reduced coverage. This is in agreement with the increase in intensity of the peaks in IR investigations [135]. At still higher temperatures, the order of the film collapses and it begins to desorb from the surface. Delamarche *et al*. [147] showed that an increase in temperature increases the tilt, which in turn reduces the effective thickness of the monolayer, and thereby generates depressions in the STM profile. Whereas MD simulations and IR investigations

suggest a decrease in tilt angle with increase in temperature, this group suggests an increase in tilt angle. They further used XPS and contact angle measurements to get the structural information of SAMs at different temperatures. From the increase in oxygen intensity as a function of temperature, oxidation of alkyl thiols to alkyl sulphonates prior to desorption has been suggested. It is to be noted that no other reports exist on the formation of sulphonates before desorption of the monolayer. The hysteresis between advancing and receding contact angles in contact angle microscopy is a measure of the surface homogeneity and order. An increase in hysteresis with temperature is reported, which reveals a severe decrease of surface order.

Poirier *et al.* proposed a two-dimensional phase diagram using variable temperature UHV STM [148]. They determined the phase stability of the decanethiol monolayer as a function of temperature and they showed that at a temperature of 300 K three phases, δ, ε and ϕ, coexist, at a still higher temperature (306 K) χ, δ and ε phases are present, these phases change to χ, ε and β at 308 K and finally, at 328 K, ε, β and α phases are present. The nature of these phases has been explained in figure 2.

2.6.7. *Thickness shear mode (TSM)*

Teuscher *et al.* used a TSM device and SERS to characterize the phase transitions in SAMs [140]. The sensitivity of TSM to both mass and viscous loading makes it ideal for characterizing changes in the structure. It is possible to understand the nature of phase transitions of SAMs by measuring the resonance frequency and impedance. The increase in resonance frequency (Δf) at higher temperature ($\sim$343 K) shows a monolayer-induced restructuring of the gold surface, which has been confirmed using conductance measurements using the oscillator at resonance. This is in agreement with the earlier STM investigations. A sudden decrease in conductance is observed at 333 K in the case of a well-ordered monolayer. This is attributed to order–disorder transitions. It has been well established that annealing results in a greater order in the monolayer structure. Conductance measurement shows a two-step transition, the first one being at 315 K and the second at 340 K. Mass spectrometric and SERS measurements confirm the absence of any oxidation product at these temperatures, suggesting that thermal disordering starts at 313–318 K. These monolayers show the conductance minimum at 333 K, above the melting point of the thiol. Thus these two transitions are attributed to a rotator-like transition and a melt-like transition. This is the first experimental evidence for the rotator-like transition; however, a two-step transition is observed in the IR investigation [133], explained as due to the untilting of the alkyl chain and a melt-like transition respectively for first and second steps.

2.7. *What do we know about phase transitions of planar monolayers?*

Various experiments suggest that SAMs are more ordered at very low temperature ($\sim$200 K). As temperature increases, alkyl chains undergo a transition from an ordered phase to another ordered phase at around 300 K. At this temperature, *gauche* defects are concentrated at the chain termini. A further increase in temperature to 318 K causes untilting of the alkyl chain. A rotator phase also has been observed at this temperature. Thermal motion of the alkyl chain causes the movement of the topmost layer of surface gold atoms. This results in the formation of vacancy islands and an ordered SAM at a reduced coverage. At still higher

temperature (~350 K), the *gauche* conformations diffuse through the middle of the chains because of the availability of free volume due to chain untilting. The alkyl chains behave like a liquid at this temperature. These experiments prove that SAMs undergo an orientational and conformational change on heating. The transition temperature varies with the chain length of the alkanethiol.

3. Monolayers on gold cluster surfaces (3D-SAMs)

As we have seen in previous sections, characterization of monolayers on planar surfaces requires more specialized techniques. The preparation of MPCs made it possible to study monolayers with conventional techniques. In the following, we give a brief review of the study of alkanethiol monolayers on gold and silver cluster surfaces and then look at their phase transitions in some detail.

Nanoclusters are molecular-like materials composed of hundreds to thousands of atoms [149, 150]. In this size regime, intermediate between a solid and a molecule, particles obey not the laws of classical mechanics, but quantum mechanics. Metal clusters with diameters up to 2 nm are also called quantum dots. Conduction electrons in these clusters feel the confinement due to low dimension and behave like a particle in a box with discrete energy states. The main fascination for very small metal clusters and their envisioned use in future electronics arise from the fact that their conduction electrons are quantized, both in number and in the states they occupy [151]. One of the important properties of these clusters is their size dependence. By precisely controlling the size and surface of a nanocrystal, its properties can be tuned. It is possible to create new nanocrystal-based materials by using the technique of molecular assembly. Nanoparticles synthesized by colloidal chemistry will tend to form non-equilibrium aggregates owing to their strong interparticle interactions [148]. In order to prevent agglomeration, these nanostructured clusters usually need to be passivated with covalently bound ligands.

A novel surfactant mediated synthesis of gold clusters was reported by Brust *et al.* [16]. These thiol-passivated nanocrystals are found to be thermodynamically stable. These monolayers are commonly known as 3D-SAMs to distinguish them from the conventional 2D-SAMs. Alkanethiols give uniform protection to the cluster surface without modification of its essential structural and electronic properties. They form compact ordered monolayers in which thiolates attach to various Au surfaces, and their spontaneous assembly is driven by the favourable van der Waals interactions. In other words, these nanocrystals are composed of a compact core of close-packed metal atoms and a dense mantle of straight chain molecules. Their chemical properties are determined by the surfactant tail group and the electronic and optical properties are characteristic of the metal particles.

3.1. *Synthesis*

The general synthetic procedure involves extraction of the metal ions from an aqueous medium to a hydrocarbon layer by means of a phase transfer reagent, followed by reduction with $NaBH_4$ in the presence of an alkanethiol [16]. After this report, various other methods were developed [152, 153]. Dialkyl sulphides have also been used as ligands, in which case the core size and polydispersity obtained were greater than for alkanethiol ligands [154]. Unsymmetrical disulphides are shown to form alkanethiol monolayers on gold cluster surfaces with 1:1 composition [155]. Porter *et al.* reported that the formation of 3D-SAMs by the adsorption of octadecyl

disulphides is distinctly different from that with octadecanethiol; the monolayer formed from the disulphide is less ordered than the thiol counterpart [156]. Less crystalline films were observed on silver clusters. In all these cases, the metal clusters behave like simple chemical compounds; they can be precipitated and redissolved. Chen *et al*. performed a time-dependent study on the cluster growth dynamics and explained how MPC core size evolves in the synthetic method [157]. They have shown that the MPC core size evolves during the first 60 h (a growth of the order of 1 nm) and remains unchanged after that. After 0.5 h, the overall average core diameter was 2.0 ± 1.1 nm, and this changed to an average core diameter of 2.6 ± 0.80 nm in 50 h. The core diameter was increased to 3.1 ± 1.4 nm after 125 h. This experiment showed that quenching of the reaction mixture during early stages of preparation will produce smaller particles [157]. Weisbecker *et al*. demonstrated that changes in the rate of flocculation of gold colloids with chemisorption of alkanethiols are pH dependent and are functions of chain length and the terminal functionality [158]. The existence of a macrocyclic effect on silver particle formation is explained using perthiolated β-cyclodextrin (β-CD) and monothiolated β-CD. The former was shown to be a more efficient capping agent [159]. Maye *et al*. have shown that heat treatment can be used for the size and shape control of nanoclusters [160]. The large surface area of these clusters leads to a higher number density of the molecules on the surface and this opens up a way to study the monolayers by conventional methodologies. The advantage of 3D-SAMs over 2D-SAMs arises here. It was suggested that, on a cluster, a majority of the atoms are on the surface and about 60% of the surface sites are occupied by the ligands [20].

Alkanethiol-protected silver clusters have been prepared using one-phase and two-phase synthetic methods [152, 161]. Electrochemical [162] as well as sono-electrochemical [163] methods of syntheses also have been reported. A number of similar nanocrystal systems have been reported in the literature [164–166]. It is found that the Au/thiol system is thermodynamically stable while others are kinetically stable [164].

3.2. *Characterization of the cluster core*

3.2.1. *Microscopy and diffraction*

Although the core dimensions for MPCs have been measured using a wide range of methodologies such as STM, AFM, transmission electron microscopy (TEM) and X-ray diffraction (XRD), TEM gives the most straightforward information on their size and shape [167]. TEM analyses suggest that the cluster core is either a truncated octahedron or a cuboctahedron. TEM measures only the core dimension, whereas STM images the total (organic + core) particle. Terrill *et al*. showed that the STM images of octadecanethiol-protected gold clusters indicate a larger radius (21 ± 1.5 Å) than TEM (only 13 Å) and they concluded that this was due to the overall cluster dimension [168].

Current–voltage characteristics of 2D Au clusters have been studied with STM and is shown to display Coulomb blockade and staircase with asymmetric behaviour [169]. Huang *et al*. showed that Coulomb blockade behaviour occurs in Au nanoclusters with a size of 9 nm, and they suggest that the alkanethiol shell is a stable tunnel barrier [170]. It is shown that the Coulomb staircase behaviour is related to MPC core size and hence the electronic structure. The double-layer capacitive charging seen for larger core sizes changes to a molecular redox-like

behaviour for small sizes. The electrostatic process or bonding interactions determine the cluster capacitance depending on the MPC core sizes [171].

Another method for the characterization of the cluster core is XRD [172, 173]. XRD not only provides definitive identification on the structure but also gives the average size of the cluster core. Evolution of the core structure with decreasing size is observed in XRD patterns. For large clusters, all the peaks are well resolved and, as the size decreases, the reflections become broader [172]. The size of the particles could be calculated from the X-ray line width broadening using the Scherrer formula for small crystalline spheres [174] ($t = k\lambda/B\cos\theta$, where k is 0.9, λ is the wavelength, B is the square root of the difference between the FWHM of the standard and that of the sample and θ is the diffraction angle of the reflection concerned). It is reported that the structure of the gold core is dependent on the diameter of the particle, where the f.c.c. structure predominates with increase in diameter [175]. XRD studies reveal the formation of a periodic arrangement of the clusters—called nanocrystalline superlattices—especially in the case of silver clusters. These superlattices are believed to be formed via the interdigitation of the alkyl chains from the adjacent clusters [176]. Small-angle X-ray scattering is particularly useful in identifying these superlattice phases [177]. We have seen that clusters with chain length above $C_n = 5$ show superlattice formation [178].

Cleveland *et al.* predicted the structures of small Au clusters with the combination of XRD, mass spectrometry and theoretical calculations [179]. They have shown that, in the size regime between 1 and 2 nm, these clusters assume a truncated decahedral structure. Extended X-ray absorption fine structure analysis of alkanethiol-protected Au clusters shows size-dependent interatomic distance contraction, but the effect is smaller than expected [180].

3.2.2. *Mass spectrometry*

One important example of core size analysis is the work reported by Schaaff *et al.* [181]. They used matrix-assisted laser desorption ionization mass spectrometry for the analysis of fractionally crystallized cluster samples in combination with TEM and theoretical calculations. This experiment suggests that the most likely shape of the gold core is a truncated octahedron. Certain magic numbers of atoms in the core are preferred. Schaaff *et al.* have shown that longer thiols form b.c.c. packing whereas shorter ones show f.c.c. packing. Arnold and Reilly calculated the number of gold and sulphur atoms using high-resolution time-of-flight mass spectrometry [182]. In this experiment, the S–C bond cleaves under UV irradiation and the Au–S fragment could be ionized and fragmented using a second laser and then mass analysed. The observed ratio of S to Au atoms suggests that sulphur atoms occupy most of the surface sites on the gold core. Murthy *et al.* used laser desorption time-of-flight mass spectrometry for the characterization of dodecanethiol-protected silver clusters, and is then compared with the size obtained from TEM and XRD [183].

3.2.3. *Nuclear magnetic resonance*

The hydrodynamic radii (R_H) of Au MPCs were determined using diffusion-controlled ordered ^{1}H NMR spectroscopy [184]. The effective average hydrodynamic radii were calculated using the Stokes–Einstein equation, $R_H = k_B T/6\pi\eta D$, at absolute temperature. These values are in agreement with the cluster sizes measured with STM. It has been shown that the corresponding edge–edge core spacings are considerably shorter than twice the length of the alkyl chains and are closer to the

single all-*trans* chain length. This result suggests that the alkyl chains undergo either interdigitation to the adjacent clusters or chain folding. Wuelfing *et al.* used Taylor diffusion coefficients to calculate the hydrodynamic diameters under different boundary conditions for the Stokes–Einstein equation. Calculated and experimental hydrodynamic diameters of MPCs in organic solvents are in good agreement to each other, implying free draining of solvent through the outer portion of the chains.

3.2.4. *Conductivity*

Solid-state conductivity measurements show that there is a distance dependence of electron transfer between Au cores, suggesting that the alkanethiol chain length influences the electronic properties of the cluster compounds [168]. From the temperature versus conductivity curve, Terrill *et al.* calculated the activation barrier energies as 9.6 ± 0.6, 16 ± 3 and $19 \pm 2\,\mathrm{kJ\,mol^{-1}}$ for the C_8, C_{12} and C_{16} clusters respectively. Recently Murray and coworkers have shown that the electronic conductivity in MPCs is due to the electron self-exchange reaction [185], where the rate of this process relates to electron tunnelling between the cores through the alkanethiol and the mixed valency of the MPC core. In this paper they concentrated on the tunnelling mechanism and the electronic conductivity of MPCs. It has been shown that there is an increase in electronic conductivity with temperature and this is due to activated electron hopping from particle to particle [186]. Silver clusters also show a similar behaviour. Fishelson *et al.* suggested the different mechanisms involved in the conduction and photoconduction of gold–dithiol nanoparticles [187]. A low effective activation energy for dark conduction is observed and is suggested to be due to the mixed mechanism of conduction, tunnelling between insulated particles and metal conduction through defects. The photoconduction mechanism involves photoemission from metal particles into the insulating layer.

3.2.5. *Absorption spectroscopy*

UV–visible absorption spectroscopy has also been used for cluster core characterization. Absorption spectroscopic measurements show the characteristic surface plasmon absorption of the metal core. Surface plasmons result from the coherent oscillation of the free electrons in the conduction band. The intensity and energy of the surface plasmon absorption depends on the core size. Bandwidth is inversely proportional to the radius r of the particles for core sizes smaller than about 20 nm [188]. For larger nanoparticles, the plasmon bandwidth increases with increasing size as the wavelength of the interacting light becomes comparable with the dimension of the nanoparticles. The broadening of the plasmon band is ascribed to retardation effects [188]. Similarly, the effect of adsorbing molecules on the electronic state of the cluster also can be seen by UV–visible spectroscopy [189]. Strongly bound ligands will dampen the plasmon band. It has been shown that the plasmon position shifts with the refractive index of the solvent and the core charge, which is in accordance with Mie theory [190]. The origin of the surface plasmon absorption and relaxation dynamics of MPCs has been described in an excellent review by Link and El-Sayed [188]. Recently Sun and Xia showed that the gold nanoshells exhibit greater sensitivity of surface plasmon resonance to environmental changes than gold solid colloids of same size [191]. Their experiment suggests that the adsorption of alkanethiol monolayers on the surface of nanoshells caused the plasmon peaks to red shift by 30 nm per methylene unit and only a 0.2 nm shift is observed for solid colloids with a mean size of 50 nm. It is also shown that the plasmon resonance of the

nanoshells can be tuned to a specific wavelength in the visible to IR range by adjusting the relative size of the dielectric core and thickness of the Au overlayer [192]. In gold clusters the surface plasmon band occurs at 520 nm, which undergoes a shift with experimental conditions such as solvents etc. In the case of silver, the surface plasmon band is at ~430 nm. He *et al.* used UV–visible spectra to study the formation process of nonanethiol-capped silver nanoclusters [193]. They have shown the formation of silver nanocrystalline superlattices. Malinsky *et al.* have explained the optical properties of silver nanoclusters by measuring the localized surface plasmon resonance (LSPR) spectra using UV–visible extinction spectroscopy [194]. They have shown that the unprotected clusters are sensitive to the external environment and their sensitivity is attenuated only by 20% when the nanoparticles are modified with long-chain alkanethiols; the LSPRs linearly shift to the red by 3 nm for every carbon atom in the alkyl chain.

3.2.6. *X-ray photoelectron spectroscopy*

X-ray photoelectron spectroscopic measurements provide information on the chemical state of the constituents [16]. XPS spectra for the carbon and sulphur regions are consistent with the presence of alkanethiolate species on Au clusters. Binding energies of the Au $4f_{7/2}$ doublet are characteristic of Au(0). The absence of the Au(I) band at 84.9 eV implies that the gold–thiol bond does not have the character of gold sulphide. Bourg *et al.* compared the S 2p (3/2) binding energies of SAMs on planar and cluster gold surfaces with those of Au(1) thiolate [195]. Their study shows that SAM systems possess a net charge of $0.2e$ and they are distinguishable from those of the thiolate. Bensebaa *et al.* showed that the S 2p binding energy is dependent on the nature of the metal and the binding energy of Au or Ag is not characteristic of the oxidized form [196]. The number of protecting ligands per cluster has been calculated using a combination of thermogravimetric data, XPS and core size analysis [168]. This gives the number of ligands per core atom and the actual coverage depends on how well the core size is known.

3.2.7. *Molecular dynamics*

MD simulations by Luedtke and Landman suggest that the structure and packing of monolayers are dependent on the finite nature of the crystallites and that the equilibrium adsorption geometry of the monolayer depends on the alkyl chain length [197]. At low temperature, the molecules are bundled into groups with a preferential parallel intermolecular orientation of the molecular backbones in each bundle, and the bundles in turn orient with respect to each other. They showed that the small clusters assume an irregular truncated octahedron morphology and sulphur atoms bind to the middle hollow site of the small (100) facets, while on the (111) facets they are arranged in a distorted hexagonal pattern with the atoms located in the middle as well as off the hollow sites as shown in figure 4. The sulphur atoms are arranged in two alternating inequivalent geometries on adjoining (111) facets with S–S distances of 3.9 and 4.5 Å. In larger clusters, the sulphur atoms are arranged in a hexagonal pattern on (111) facets, with the centre atom being the on-top site, and on the (100) facet they form a rhombus with the atoms adsorbed off the hollow sites. The S–S distances in these clusters are 4.1 Å (on the (100) facets) and 4.3 Å (on the (111) facets). The nearest-neighbour distance between Au atoms is ~2.8 Å. These distances suggest around a 12% contraction of the mean nearest-

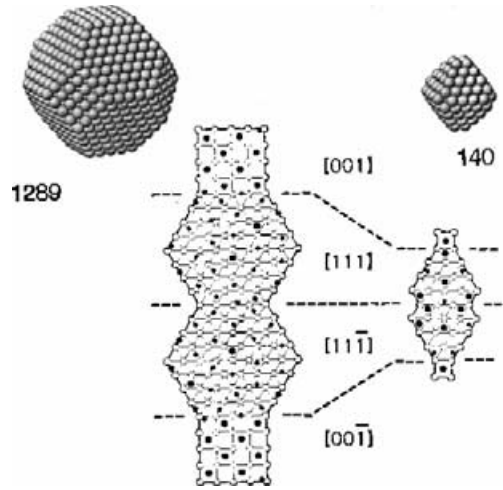

Figure 4. Arrangement of the sulphurs (full circles) on the facets (gold atoms are shown as open circles) of the equilibrium structures of $Au_{140}(TO)^+$ and $Au_{1289}(TO)$ nanocrystallites, at right and left respectively. (From Ludtke and Landman [205].)

neighbour distance between adsorbed sulphur atoms compared with planar Au (111) surfaces, which results in a ~30% increase in their packing density.

Van Hyning *et al.* have given a mechanism for the growth of 5–30 nm silver nanoclusters [198]. They have shown that, within 5 s of mixing the metal salt and the reducing agent, reduction takes place resulting in the formation of a 2.5 nm cluster. Followed by this, an aggregative growth mechanism is suggested.

3.3. *Characterization of monolayers*

3.3.1. *Nuclear magnetic resonance*

The structure of alkanethiolate monolayers in MPC solids has been probed by ^{13}C NMR [168] and transmission IR [199] spectroscopies. ^{13}C NMR focuses on the dependence of chemical shifts as a function of the carbon position relative to the gold–hydrocarbon interface. Figure 5 shows the ^{13}C NMR spectra of octanethiol monomer and octanethiolate-, dodecanethiolate- and hexadecanethiolate-protected Au clusters. The important findings here are, compared with the C_8 monomer and cluster, that all the peaks are broadened in the cluster, attributed to the immobilization of the surfactant on the cluster surface. Going from the shorter to longer chain lengths, the peak width narrows, as the carbon is located further away from the thiol functionality. Other significant observations are that the resonances from carbon atoms closest to the Au core, those due to C_α, C_β and C_γ, are broadened into the baseline and that there is a systematic change in both the chemical shift and the line width with the carbon position relative to the Au–hydrocarbon interface. These are attributed to the discontinuity in the diamagnetic susceptibility at the Au–hydrocarbon interface and residual dipolar interactions in alkanethiolate monolayers. Badia *et al.* compared the adsorption of thiols on a cluster surface with that of Au(1) alkyl thiolates and found that the chemisorbed species on the gold nanoparticle surface is a thiolate, not a disulphide [200]. They observed a line broadening of the C_1 and C_2 sites, which is explained as due to the chemical shift

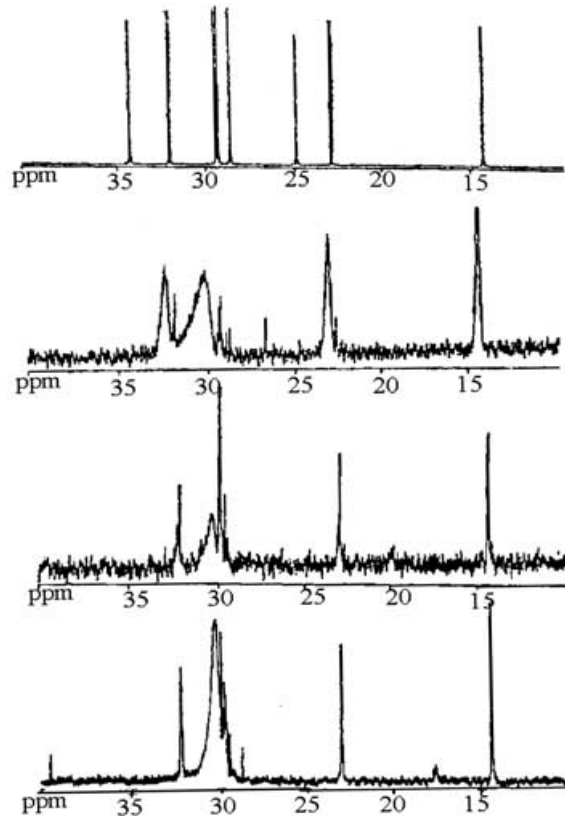

Figure 5. ^{13}C NMR spectra of (*a*) octanethiol monolayer and Au clusters protected with (*b*) octanethiol, (*c*) dodecanethiol and (*d*) hexadecanethiol. C_n represents the position of carbon from the surface. (From Terrill *et al.* [168].)

distribution resulting from the different adsorption sites and/or non-spherical particle shapes. These observations show the similarity of these 3D-SAMs to the corresponding 2D-SAMs. NMR data suggest that the long alkyl chain surfactant on gold nanoclusters is in a semicrystalline state. At room temperature, all-*trans* chains coexist with a smaller population of more mobile chains containing *gauche* conformers [168]. The shorter-chain thiols are disordered even at room temperature. Broadening of the resonances as well as the disappearance of the carbons closest to the surface shows the immobilization of the alkyl chains and the strong interaction with the metal surface respectively. The upfield shift of C_{17} in $C_{18}S$–Au and the Gaussian decay of the signal in the dipolar dephasing experiments suggest the presence of a motionally restricted interior of the alkyl chain and the conformationally disordered chain ends. The methyl proton line widths are lower than those of crystalline alkanes, suggesting that large-amplitude motions are taking place about the chain axis.

3.3.2. *IR spectroscopy*

A comprehensive IR spectroscopic study of monolayers on nanoclusters has been carried out by Hostetler *et al.* [199]. An increase in intensity of the methylene stretching vibrations with chain length indicates that structural integrity of the

alkanethiol was maintained during the cluster formation. Another important aspect is the position of the methylene symmetric and asymmetric stretching modes. For crystalline *n*-alkanes, these values are at 2850 and 2920 cm^{-1}; for liquids, they are at 2856 and 2928 cm^{-1} respectively [85]. All alkanethiolate monolayers above $n = 8$ show crystalline order while below this a liquid-like state is observed. This behaviour was shown by RAIRS of 2D-SAMs as well. In the low-frequency region, the presence of progression bands as a series of well-resolved peaks is again a strong indication of crystallinity. The essential conclusions drawn from IR investigations are that (1) thiol is adsorbing on the surface by dissociative chemisorption, (2) the majority of the alkanethiolate ligands are in an all-*trans* zigzag conformation and (3) there is a structural resemblance to the monolayers on flat gold surfaces.

We have studied alkanethiols on silver clusters by IR spectroscopy [178]. The presence of d^+ and d^- modes at 2850 and 2920 cm^{-1} in the case of long-chain alkanethiols ($n = 8$) shows the crystalline-like environment. Short-chain alkanethiols shows liquid-like behaviour. The absence of S–H stretching indicates the loss of thiolate proton on adsorption. It has been shown that a repeated heating–cooling cycle (up to a temperature of 473 K) results in the annealing of the monolayer on the surface [137].

We measured mass spectra of the desorbed alkane thiols from the Au and Ag clusters [178]. In all cases, we saw the peaks due to R^+, RS^+, $RSSH^+$ and $(RS)_2$, which are characteristic signatures of the thiol mass spectrum. From the absence of the disulphide band in the IR spectra, we attribute the $(RSSH)^+$ and $(RS)_2$ peaks to ion/molecule reactions on desorption. All the desorptions occur at approximately 550 K, close to the value obtained from thermogravimetric analysis.

3.4. *Essential aspects of the structure of MPCs*

Nanometre-scale metal clusters have found potential for a variety of applications ranging from electronic devices and sensors to catalysis. In order to preserve their size, these metal clusters need to be passivated. Thiol-passivated metal clusters of Au and Ag have been attractive to various groups. It has been shown that each molecule of an MPC has a compact, crystalline metal core of 1–4 nm size, which is encapsulated within a shell of tightly packed hydrocarbon chains linked to the core via the sulphur atoms. The precise structure of the core is still unknown, but theoretical and experimental evidence suggests that it is faceted. The electronic and optical properties are intensely structured, showing the effects of conduction level quantization of a metallic $Au^{(0)}$ or $Ag^{(0)}$ core, and the electrical conduction is by single-electron tunnelling, which results in a Coulomb staircase pattern in the redox waves [201, 202]. XPS, IR and NMR analyses suggest that it is the thiolate which is present on the surface. IR studies confirm a fully ordered crystalline all-*trans* arrangement of the long-chain alkanethiols, whereas the short-chain thiols are liquid like. The absence of S–H stretching in IR indicates that the alkyl thiols adsorb on gold/silver by losing the proton. Recently Hasan *et al.* showed the presence of intact thiols on MPCs [203]. They have used a ligand exchange reaction of dodecyl sulphide with thiols and showed the presence of thiol in NMR. Later the thiol undergoes a slow proton exchange reaction. TEM and XRD measurements show that the adjacent Au particles are separated by approximately one chain length, not the expected two chain lengths. This suggests that the long-range ordering arises from the interdigitation of chain domains on neighbouring particles. Mirkin and coworkers studied the properties of DNA-modified nanoparticles [204] and have

shown that the optical properties of DNA-linked nanoparticle assemblies are governed by their aggregate size. They have shown that the aggregate growth is through an 'Ostwald ripening' mechanism.

It has been shown that the thiolate chains undergo melting at higher temperature than in 2D-SAMs. In the next section we review the phase behaviour of these monolayers on cluster surfaces as a function of temperature.

3.5. *Phase transitions of monolayers in MPCs*

3.5.1. *MD simulations*

MD simulations suggest that the monolayers undergo a phase transition near the bulk melting temperature of the alkane residue of the corresponding alkyl thiolate, accompanied by intramolecular conformational changes [205]. They predicted a first-order phase transition for both the short-chain and the long-chain monolayers, with the melting temperatures close to that of the corresponding alkyl chain melting temperature, while experimental observations as well as SAMs on planar surface suggest that long-chain alkyl thiols melt around 333 K. The melting transition results in changes in the intermolecular structure, that is from the bundled state to a disordered state. The melting temperature depends on the chain length of the passivating thiol as well as the cluster core size. It has been shown that the outer boundary chains start to develop *gauche* defects at lower temperature than the chains near to the core. At high temperature, these defects progress towards the interior and, after the melting point, both the outer and the interior chains appear the same [205]. This is clear from DSC, variable temperature IR and NMR measurements as discussed below.

3.5.2. *Differential scanning calorimetry*

Phase transitions in alkanethiolate monolayers on gold clusters have been detected by DSC [206], variable temperature NMR and variable temperature IR spectroscopies [207]. Melting points and phase transitions of the materials as well as the enthalpic changes can be measured with DSC. All the clusters with chain lengths more than 8 show a broad endotherm in DSC at 330 K, indicating a phase transition. This transition is attributed to melting of the alkyl chains. In clusters, because of the high curvature of the surface, the chain termini of the alkyl groups are more diverged than the head group. This causes the interpenetration of the adjacent alkyl chain termini into this gap and the van der Waals forces make this structure more ordered and stable. The observed transition is attributed to the melting of the alkyl chains in the interdigitated regions. Enthalpy associated with the transition increases with increasing chain length, because larger chain length affords more extensive van der Waals interactions and resulting enthalpic contributions. Badia *et al.* used variously deuterated octadecanethiolate monolayers for understanding the nature of the phase transition [207]. The broad endotherm present in DSC suggests a thermally induced reversible phase transition. Figure 6 shows the DSC traces of deuterated alkanethiols. The peak maximum temperature for 1,1-d_2-C_{18}SAu and d_{35}-C_{18}SAu are 316 and 328 K respectively. This difference suggests that the chain melting begins at the chain terminus and propagates towards the centre of the chain as the temperature increases. This result has been confirmed with FTIR and ^{2}H NMR studies.

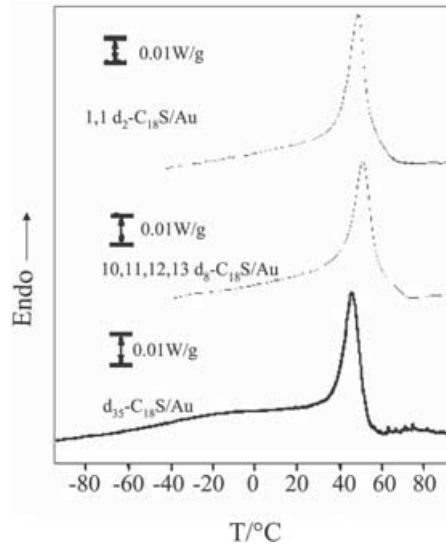

Figure 6. DSC traces of deuterated alkanethiol monolayers. Presence of an endotherm of >40°C indicates alkane chain melting. (From Badia *et al.* [206].)

3.5.3. *Nuclear magnetic resonance*

Variable temperature NMR experiments suggest that as temperature increases the disordering of the alkyl chains increases. The transition temperature range is similar to that observed by DSC. The degree of conformational order depends on the particle size and the nature of the terminal group in addition to the chain length. Evolution of a peak at 31 ppm in the solid-state variable temperature ^{13}C NMR spectra of C_{14} and C_{18} clusters shows a phase transition [208]. This peak is assigned to the conformationally disordered chains. As the chain length increases from C_{14} to C_{18}, the transition temperature increases from 297 to 318 K. In contrast to the long-chain samples, when the C_8S–Au sample was heated to 323 K, the only changes observed were a slight narrowing and a small upfield shift of the peaks, confirming that the short chains are already in a liquid-like state at 298 K. Deuterium NMR studies reveal that the phase transition is due to an increased frequency of the *gauche* conformations, caused by an increase in the free chain volume. This in turn results in the pseudo-rotational motion of the individual chain segments about the long axis of the RS chain segments including both axial rotation and rapid bond isomerization. From the difference in patterns of the 1,1-d_2-C_{18}SAu and other samples, they concluded that there is no measurable degree of *trans–gauche* bond isomerization in the vicinity of C_1–C_2 bond, and the axial rotation about the C–S bond is unlikely.

When the alkyl thiols contain terminal groups such as hydroxyl or carboxyl, the transition temperature is found to be higher than that of the methyl-terminated thiols. This is due to the formation of hydrogen bonding, which gives higher order and increased thermal stability. The hydrogen bond induces a greater degree of conformational order at room temperature, which does not occur easily via van der Waals interaction alone. Schmitt *et al.* carried out a comprehensive study of the phase transition of carboxyl-terminated alkanethiol-protected gold clusters [209]. They found that at room temperature these alkyl thiols are all-*trans* and are in a thermally stable, motionally restricted state with chain melting observed only above

413 K. This is in contrast to the behaviour of methyl- or hydroxyl-terminated thiols, where a chain length dependent transition is observed at a lower temperature [208]. Schmitt *et al*. observed a strong thermal hysteresis in these thiols that is attributed to the change in the hydrogen bonding network from 2D (intramolecular) like to 3D (intermolecular) like.

3.5.4. *IR spectroscopy*

IR studies show that monolayers undergo a transition from an ordered state to a disordered state at the phase transition temperature [206]. The methylene stretching modes were shifted from solid-like to liquid-like values at higher temperatures. However, no insight was gained concerning where the disordering starts and how far along the chain the disorder propagates. This can be explained using deuterium labelling. In the experiment, *n*-octadecanethiol deuterated at different positions along the alkyl chain was used [207]. The molecules are $CD_3(CD_2)_{16}CH_2SH$ (positions 2–18 are deuterated), referred to as d_{35}-C_{18}, $CH_3(CH_2)_{16}CD_2SH$ (position 1 is deuterated), referred to as d_2-C_{18}, and $CH_3(CH_2)_4(CD_2)_4(CH_2)_9SH$ (positions 10–13 are deuterated), referred to as d_8-C_{18}. In d_8-C_{18}, a sudden transition is observed at the phase transition temperature (318 K) whereas, in d_{35}-C_{18}, the shift is gradual, which is due to the gradual increase in amount of the *gauche* conformer. These two experiments show that melting commences at the chain terminus and propagates towards the middle of the chain with increasing temperature. In the case of d_2-C_{18}, there is no shift in the temperature range 283–373 K. This suggests that local order is maintained at the carbon closest to the Au surface during the chain disordering transition.

We measured variable temperature IR of alkanethiol-protected Au and Ag clusters [137]. The d^+ and d^- modes show a blue shift with increase in temperature. This suggests the melting of the alkyl chain. IR spectra of octadecanethiol-protected Ag clusters at different temperatures are shown in figure 7. This transition appears to be reversible up to 473 K, which is confirmed by DSC. In the repeated cycles, an increase in enthalpy of this transition is observed and is more pronounced in Ag clusters. *Ex situ* IR measurements [137] of the sample (after heating–cooling cycles) show the splitting of the methylene scissoring and rocking modes, which is an indication of more ordered structure [210]. This is attributed to the annealing of the monolayer on the surface. In the temperature-dependent IR spectra of monolayers on planar surfaces, the methylene scissoring mode splits into two at 80 K, which is explained as due to annealing of the monolayer [211].

Shape transformation of the cluster core has been observed at higher temperatures in TEM measurements [212]. Removal of the surface capping polymer followed by a small truncation occurred in the particles in the temperature range 453–727 K. The particle shapes change dramatically to a near-spherical geometry when the temperature range is above 773 K. It has been shown that tetrahedral particles are more stable than cubic ones, possibly because of the lower surface energy of the (111) surface than the (100) surface.

3.5.5. *Neutron scattering*

Neutron scattering is a powerful technique [213] to study the dynamics in condensed matter, as the energy of thermal neutrons matches the energy of the system. Because of the large cross-section of protons, alkanes (hence alkanethiols) are more suitable for neutron scattering studies. The random motion of the particles

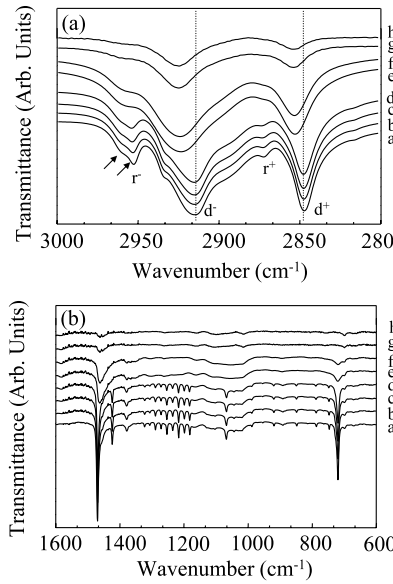

Figure 7. Variable temperature IR spectra of the (*a*) high- and (*b*) low-frequency regions for the $C_{18}S$-Ag nanoparticle. spectra a, b, c, d, e, f, g and h correspond to 298, 323, 348, 373, 398, 423, 448 and 473 K respectively. Arrows show the splitting of the r^- band which is an indication of the frozen alkyl chain end. (From Sandhyarani *et al.* [137].)

in the system leads to Doppler broadening of the scattered neutrons which results in the broadening of the elastic line known as quasi-elastic neutron scattering (QENS). QENS not only provides the time scale but also the geometry of motions. Recently we have shown that the dynamics of alkanethiols on Au or Ag cluster surfaces can be monitored by neutron scattering [214]. At 340 K and above, quasi-elastic (QE) broadening is observed in the octadecanethiol-protected Au clusters, which is explained as due to the melting of the alkyl chain. Figure 8 shows the QENS spectra for octadecanethiol-protected silver clusters (Ag-ODT) at room temperature taken with two instrumental resolutions [215]. No QE broadening was observed corresponding to dynamically frozen alkyl chains. However, as the temperature is increased, the spectra begin to show QE broadening. This evolution of dynamics is dependent on chain length. It has been found that the principal rotational motion of the chains is the uniaxial motion, and the observed dynamics can be well represented with six-fold jump diffusion. The study suggests that the alkyl chains are held rigidly and the interchain distance is 4.4 Å, suggesting closest packing of chains resulting in larger coverage than the planar monolayers. It has been shown that, while cooling, QE broadening is observed even at 300 K, which is suggested to be due to hysteresis.

3.6. *Essentials of phase transitions of monolayers in MPCs*

Monolayers on gold and silver cluster surfaces are shown to undergo phase transition at higher temperatures. This solid–liquid phase transition is monitored by DSC, variable temperature IR and NMR spectroscopes. The energetics of the transition depends on the chain length of the thiol as well as the size of the cluster core. Detailed analysis using deuterium labelling shows that melting starts from the

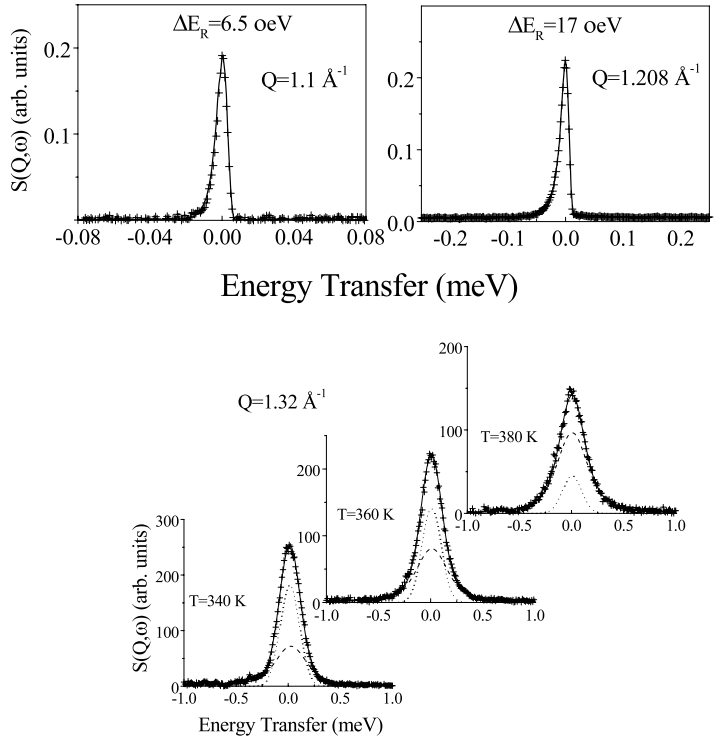

Figure 8. QENS spectra of Ag-ODT sample at room temperature taken using a high resolution instrument (top). No QE broadening over the resolution of the instrument is observed. Points are data and full curves correspond to the resolution function of the instrument. QENS spectra of Ag-ODT at different temperatures using a different QENS spectrometer (bottom). The evolution of the dynamical motion with temperature is evident with the increase QE component. Points are data and dotted and broken curves are elastic and QE components respectively. [From Mukhopadhyay *et al.* [215].]

top of the alkyl chain (methyl group in alkanethiols) and progresses towards the surface methylene groups. A neutron scattering study shows that rotational dynamics is absent at room temperature at least for longer chain length monolayers and evolves with increase in temperature.

3.7. *Stability of monolayers in MPCs*

The stability of monolayers on the cluster surface is an important issue to be taken care of in their preparation and storage. Studies suggest that MPCs are stable in air at room temperature for extended periods of time (of the order of 6 months). Recently we have shown that ozone can oxidize the monolayer as in the 2D-SAMs [216]. The sulphur head group becomes oxidized and this results in desorption of some of the molecules as evidenced by the loss of intensity of CH modes in the IR spectrum. This results in the aggregation of the clusters. We have also demonstrated radical-induced core destruction and desorption of the monolayer [217]. In the presence of UV light and chlorinated solvents, the monolayer desorbs from the surface in the form of partially halogenated disulphides. We observed the radical-induced etching of gold in 2D-SAM also but with a low rate. Both Au and Ag

clusters in solution are reactive to halocarbons. Extensive studies suggest that the process is a catalytic mineralization resulting in the complete destruction of the halocarbon, forming amorphous carbon [218]. It is shown that heating the MPC to higher temperature (<623 K) produces core metal films [219]. Schaaff *et al*. demonstrated the etching of Au atoms from the outermost surface layer of the cluster core, when heated in neat dodecanethiol solution under an inert atmosphere. This experiment suggests that the thiol acts both as efficient stabilizer and as an etchant [220]. Photon-initiated shape transformation and fragmentation of alkanethiol-coated gold and silver clusters have been reported. Silver particles show fragmentation and gold barely does so, and the difference in the behaviour of these two metals is attributed to the differences in work function, oxidation potential, atomization enthalpy and particle size [221].

4. Comparison between SAMs on 2D and 3D surfaces

Metal nanoparticles are highly faceted with (111) and (100) faces and hence the monolayers on them can be compared with those on planar surfaces. Various studies suggest that there is an excellent correspondence between the chain length dependent order–disorder phase transitions observed in the two systems. There is a higher alkanethiolate surface density on the nanoparticles (15.4 $Å^2$/molecule) than on the flat Au (111) surface (21.4 $Å^2$/molecule). The greater concentration of surface defect sites and the high radius of curvature of the cluster allow a larger proportion of the gold atoms on the cluster surface that in turn results in the greater coverage of the monolayers on the surface. The SAMs on nanocrystallites exhibit a greater packing density, where the ratio of the number of exposed gold atoms to the number of exposed sulphur atoms is between 1.55 and 1.87 in smaller and larger crystallites respectively. This ratio is 3 in SAMs on a planar gold surface. This would mean a high density of the monolayers near the cluster surface and a large decrease near the terminal CH_3 group. This results in the greater mobility of the terminal group.

Alkanethiols form $(\sqrt{3} \pm \sqrt{3})$ R30° and $c(4 \times 2)$ structures on the Au (111) surface, whereas on Au (100) there is a distorted hexagonal arrangement with $c(2 \times 8)$ unit cell structure. Sulphur atoms assume a hexagonal geometry on the Au (111) surface. The S–S distance is 4.97 Å on Au (111) and 4.54 Å on Au (100). The S–S distance in Ag (111) is 4.41 Å, which is close to the interchain repeat distances in crystalline alkanes. The greater distance on Au (111) makes the monolayer tilt around 30° from the surface normal. The closer values for Au (100) and Ag (111) to the solid alkane distance causes the monolayers on these surfaces to have a more perpendicular geometry (~5° tilt with respect to the surface normal). The arrangement of molecules on the nanocrystalline surface depends on the size of the nanocrystallites. In smaller crystallites the sulphur binds in the middle hollow site of the (100) facets and a distorted hexagonal arrangement occurs on Au (111) facets. In larger nanocrystallites sulphurs are arranged on the (100) facets in a $c(2 \times 2)$ pattern on hollow sites and on the (111) facets they form a hexagonal pattern. In small clusters the sulphur atoms are arranged in two alternating inequivalent geometries on adjoining (111) facets with S–S distances of 3.9 and 4.5 Å. In large clusters, sulphur atoms are in a hexagonal geometry on (111) facets as in the case of the planar (111) surface. It is shown that, at low temperature, the alkanethiol molecules are bundled into groups with parallel intermolecular orientations of the

molecular backbones in each bundle; the bundles in turn are preferentially oriented with respect to each other.

In both 2D- and 3D-SAMs, alkanethiols take a fully all-*trans* zigzag conformation with *gauche* defects concentrated at the chain termini. The defect concentration increases with increasing temperature and decreases with increasing pressure. Studies established that in both planar and cluster surfaces longer alkanethiols ($n > 9$) assume a crystalline well-packed arrangement, whereas shorter-chain thiols show liquid-like behaviour. This is due to the increased van der Waals interaction in the longer-chain alkanethiols. Kinetic study of 2D monolayers establishes a two-step mechanism for their formation, whereas such studies do not exist for monolayers on a cluster surface. Both 2D- and 3D-SAMs are stable in air and they undergo oxidation in the presence of ozone. The rate of oxidation is faster on cluster surfaces, probably because of the better penetration of O_2 or O_3 through the alkane chains on cluster surfaces as a result of their curvature.

Alkanethiol monolayers on planar and cluster surfaces undergo melting prior to desorption. The temperature is dependent on the chain length of the thiol; longer thiols melt at higher temperature owing to the increased van der Waals interaction. In the case of a cluster surface, this also depends on the size of the cluster. The melting temperature is higher in larger clusters. As in the planar surface, a higher melting temperature is reported for longer chains. The transition temperature is greater than the melting point of the bulk thiol. There is a higher degree of order in the monolayers relative to the bulk materials, and this is due to the restriction imposed by the Au–S bond. Studies show that the melting transition is first order. Various studies of 2D-SAMs clearly demonstrate the existence of more than one transition, whereas such information is not available for SAMs on cluster surfaces. Only one melting transition is observed in the latter. It is reported that the outer boundary chains of the bundle (of alkane chains) melt first and then the chains inside the bundle. In both of these 2D- and 3D-SAMs, the melting of monolayer starts on the terminal group and proceeds inward. The energetics of transition in 3D-SAMs is well established, whereas not much is known about the energetics of the transition in 2D-SAMs.

5. Conclusions

This review has looked at some of the key issues concerning the structure and phase transitions of monolayers. It is evident that there are significant similarities between the 2D and 3D monolayer systems, but there are also distinct differences both in terms of the packing density and in terms of the origin and propagation of conformational defects. It is clear that most of the alkyl chains form bundles on the various planes on the nanocrystal surfaces and there is very little rotational dynamics present in them at room temperature. The literature presents a consistent picture of the monolayer structure, yet there are no definite data on issues such as energetics. Certain aspects such as structure and phase behaviour of the monolayers as a function of core dimension need to be looked at.

Acknowledgements

T.P. thanks the Department of Science and Technology and Council of Scientific and Industrial Research, Government of India, for supporting his research

programme on monolayers. He also thanks the students and collaborators who have contributed to the work presented.

References

[1] Langmuir, I., 1917, *J. Am. Chem. Soc.*, **39**, 1848.
[2] Franklin, B., 1774, *Philos. Trans. R. Soc.*, **64**, 445.
[3] Pockels, A., 1891, *Nature*, **43**, 437.
[4] Petty, M. C., and Barlow, W. A., 1990, Film deposition, *Langmuir–Blodgett Films*, edited by G. Roberts (New York: Plenum), pp. 93–123.
[5] Blodgett, K. B., 1935, *J. Am. Chem. Soc.*, **57**, 1007.
[6] Bigelow, W. C., Picket, D. L., and Zisman, W. P., 1946, *J. Colloid Interface Sci.*, **1**, 513.
[7] Nuzzo, R. G., and Allara, D. L., 1983, *J. Am. Chem. Soc.*, **105**, 4481.
[8] Sagiv, J., and Taya, K., 1980, *J. Am. Chem. Soc.*, **102**, 92–98.
[9] Ogawa, H., Chihera, T., and Taya, K., 1985, *J. Am. Chem. Soc.*, **107**, 1365.
[10] Ulman, A., 1991, *An Introduction to Ultrathin Organic Films: from Langmuir Blodgett to Self-Assembly* (New York: Academic).
[11] Kepley, L. J., Crooks, R. M., and Ricco, A. J., 1992, *Anal. Chem.*, **64**, 3191.
[12] Yamamoto, Y., Nishihara, H., and Aramaki, K., 1993, *J. Electrochem. Soc.*, **140**, 436.
[13] Häussling, L., Michel, B., Ringsdorf, H., and Rohrer, H., 1991, *Angew. Chem., int. Edn. Engl.*, **30**, 569.
[14] Frostman, L. M., Bader, M. M., and Ward, M. D., 1994, *Langmuir*, **10**, 576.
[15] Allara, D.L., 1995, *Biosens. Bioelectron.*, **10**, 771–783.
[16] Brust, M., Walker, M., Bethell, D., Schiffrin, D. J., and Whyman, R., 1994, *J. Chem. Soc., Chem. Commun.*, 801–802.
[17] Ulman, A., 1996, *Chem. Rev.*, **96**, 1533–1554.
[18] Poirier, G. E., 1997, *Chem. Rev.*, **97**, 1117–1127.
[19] Schreiber, F., 2000, *Prog. Surf. Sci.*, **65**, 151–256.
[20] Hostetler, M. J., and Murray, R. W., 1997, *Curr. Opin. Colloid Interface Sci.*, **2**, 42–50.
[21] Templeton, A. C., Wuelfing, W. P., and Murray, R. W., 2000, *Acc. chem. Res.*, **33**, 27–36.
[22] Anderson, M. R., Evanik, M. N., and Zhang, M., 1996, *Langmuir*, **12**, 2327–2331.
[23] Xiao, X. D., Wang, B., Zhang, C., Yang, Y., and Loy, M. M. T, 2001, *Surf. Sci.*, **472**, 41–50.
[24] Heister, K., Allara, D. L., Bahnck, K., Frey, S., Zharnikov, M., and Grunze, M., 1999, *Langmuir*, **15**, 5440–5443.
[25] Porter, M. D., Bright, T. B., Allara, D. L., and Chidsey, C. E. D., 1987, *J. Am. Chem. Soc.*, **109**, 3559–3568.
[26] Meuse, C. W., 2000, *Langmuir*, **16**, 9483–9487.
[27] Shi, J., Hong, B., Parikh, A. N., Collins, R. W., and Allara, D. L., 1995, *Chem. Phys. Lett.*, **246**, 90–94.
[28] Ehler, T. T., Malamberg, N., Carron, K., Sullivan, B. P., and Nee, J., 1997, *J. phys.Chem.* B, **101**, 3174–3180.
[29] Chechik, V., Schonher, H., Vansco, G. J., and Stirling, C. J. M., 1998, *Langmuir*, **11**, 3003–3010.
[30] Kajikawa, K., Hara, M., Sasabe, H., and Knoll, W., 1997, *Jpn. J. Appl. Phys.* B, **8**, L1116–L1119.
[31] Peterlinz, K. A., and Georgiadis, R., 1996, *Langmuir*, **12**, 4731–4740.
[32] Nelson, B. P., Frutos, A. G., Brockman, J. M., and Corn, R. M., 1999, *Anal. Chem.*, **71**, 3928–3934.
[33] Ehler, T. T., Malmberg, N., and Noe, L. J., 1997, *J. phys. Chem.* B, **101**, 1268–1272.
[34] Shuck, P., 1997, *Annu. Rev. phys. Chem.*, **26**, 541–566.
[35] Brockman, J. M., Nelson, B. P., and Corn, R. M., 2000, *Annu. Rev. phys. Chem.*, **51**, 41–63.

[36] Dannenberger, O., Buck, M., and Grunze, M., 1999, *J. phys. Chem.*, **103**, 2202–2213.
[37] Buck, M., Grunze, M., Eisert, F., Fischer, J., and Trager, F., 1992, *J. Vacuum. Sci. Technol.* A, **10**, 926–929.
[38] Zhang, Y., Zhang, Y., Terrill, R. H., and Bohn, P. W., 1998, *Thin Solid Films*, **335**, 178–185.
[39] Buscher, C. T., McBranch, D., and Li, D., 1996, *J. Am. Chem. Soc.*, **118**, 2950–2953.
[40] Beard, B. C., and Brizzolara, R. A., 1996, *J. Vac. Sci. Technol.* A, **14**, 89–94.
[41] Bindu, V., and Pradeep, T., 1998, *Vacuum*, **49**, 63.
[42] Ishida, T., Nishida, N., Tsuneda, S., Hara, M., Sasabe, H., and Knoll, W., 1998, *Jpn. J. appl. Phys.* B, **12**, L1710–L1713.
[43] Ishida, T., Hara, M., Kojima, I., Tsuneda, S., Nishida, N., Sasabe, H., and Knoll, W., 1998, *Langmuir*, **14**, 2092–2098.
[44] Yang, D. Q., Sun, Y., and Da, D. A., 1991, *Appl. Surf. Sci.*, **145**, 451–455.
[45] Heister, K., Zharnikov, M., Grunze, M., and Johansson, L. S. O., 2001, *J. phys. Chem.* B, **105**, 4058–4061.
[46] Himmelhaus, M., Gauss, I., Buck, M., Eisert, F., Woll, C., and Grunze, M., 1998, *J. Electron Spectrosc. relat. Phenom.*, **92**, 139–149.
[47] Zubragel, C., Deuper, C., Schneider, F., Neumann, M., Grunze, M., Schertel, A., and Woll, C., 1995, *Chem. Phys. Lett.*, **238**, 308–312.
[48] Miller, W. J., and Abbot, N. L., 1997, *Langmuir*, **13**, 7106.
[49] Laibinis, P. E., Fox, M. A., Folkers, J. P., and Whitesides, G. M., 1991, *Langmuir*, **7**, 3167–3173.
[50] Hatt, D. A., and Legget, G. J., 1999, *J. mater. Chem.*, **9**, 923–928.
[51] Mohri, N., Matsushita, S., and Inour, M., 1998, *Langmuir*, **14**, 2343.
[52] Noh, J., Hara, M., and Knoll, W., 1999, *Mol. Cryst. Liq. Cryst.*, **337**, 161–164.
[53] Kondoh, H., Kodama, C., Sumida, H., and Nozoye, H., 1999, *J. chem. Phys.*, **111**, 1175–1184.
[54] Strong, L., and Whitesides, G. M., 1988, *Langmuir*, **4**, 546.
[55] Chidsey, C. E. D., and Loiacono, D. N., 1990, *Langmuir*, **6**, 709.
[56] Dubois, L. H., Zegarski, B. R., and Nuzzo, R. G., 1993, *J. chem. phys.*, **98**, 678–688.
[57] Balzer, F., Gerlach, R., Polanski, G., and Rubahn, H. G., 1997, *Chem. Phys. Lett.*, **274**, 145–151.
[58] Chidsey, C. E. D., Liu, G.-Y., Rowntree, Y. P., and Scoles, G., 1989, *J. Chem. Phys.*, **91**, 4421–4423.
[59] Weiss, P. S., 1996, *J. Am. Chem. Soc.*, **118**, 934.
[60] Noy, A., Vezenov, D. V., and Lieber, C. M., 1997, *Annu. Rev. mater. Sci.*, **27**, 381–421.
[61] Camillone, N., Eisenberger, P., Leung, T. Y. B., Schwartz, P., Scoles, G., Poirier, G. E., and Tarlov, M. J., 1994, *J. chem. Phys.*, **12**, 11031–11036.
[62] Umezawa, Y., 1997, *Langmuir*, **13**, 4323–4332.
[63] Poirier, G. E., 1996, *J. Vac. Sci. Technol.* B., **14**, 1453–1460.
[64] Schweizer, M., Hagenstrom, H., and Kolb, D. M., 2001, *Surf. Sci.*, **490**, L627–L636.
[65] Arce, F. T., Vela, M. E., Salvarezza, R. C., and Arvia, A. J., 1998, *Langmuir*, **14**, 7203–7212.
[66] Poirier, G. E., 1999, *Langmuir*, **15**, 1167–1175.
[67] Heinz, R., and Rabe, J. P., 1995, *Langmuir*, **11**, 506–511.
[68] Alves, C. A., Smith, E. L., and Porter, M. D., 1992, *J. Am. Chem. Soc.*, **114**, 1222–1227.
[69] Noh, J., Nakajima, K., Hara, M., Sasabe, H., Knoll, W., and Lee, H., 1998, *Korea Polym. J.*, **6**, 307–311.
[70] Arce, F. T., Vela, M. E., Salvarezza, R. C., and Arvia, A. J., 1998, *Electrochim. Acta*, **44**, 1053–1067.
[71] Alves, C. A., and Porter, M. D., 1993, *Langmuir*, **9**, 3507–3512.
[72] Tamada, K., Hara, M., Sasabe, H., and Knoll, W., 1997, *Langmuir*, **13**, 1558–1566.
[73] Doudevski, I., and Schwartz, D. K., 2000, *Langmuir*, **16**, 9381–9384.

[74] Fenter, P., Eisenberger, P. O., and Liang, K. S., 1993, *Phys. Rev. Lett.*, **70**, 2447–2450.
[75] Fenter, P., Eisenberg, P., Li, J., Chemillone, N., Bernasek, S., Scoles, G., Ramanarayanan, T. A., and Liang, K. S., 1991, *Langmuir*, **7**, 2013
[76] Porter, M. D., Bright, T. B., Allara, D. L., and Chidsey, C. E. D., 1987, *J. Am. Chem. Soc.*, **109**, 3559–3568.
[77] Diao, P., Jiang, D. L., Cui, X. L., Gu, D. P., Tong, R. T., and Zhong, B., 1999, *J. electroanal. Chem.*, **464**, 61–67.
[78] Hagenstrom, H., Schneeweiss, M. A., and Kolb, D. M., 1999, *Langmuir*, **15**, 2435–2443.
[79] Mohtat, N., Byloos, M., Soucy, M., Morin, S., and Morin, M., 2000, *J. Electroanal. Chem.*, **484**, 120–130.
[80] Boubour, E., and Lennox, R. B., 2000, *J. phys. Chem.* B, **104**, 9004–9010.
[81] Hatchett, D. W., Uibel, R. H., Stevenson, K. J., Harris, J. M., and White, H. S., 1998, *J. Am. Chem. Soc.*, **120**, 1062–1069.
[82] Nuzzo, R. G., Dubois, L. H., and Allara, D. L., 1990, *J. Am. Chem. Soc.*, **112**, 558.
[83] Laibinis, P. E., Whitesides, G. M., Allara, D. L., Tao, Y. T., Parikh, A. N., and Nuzzo, R. G., 1991, *J. Am. Chem. Soc.*, **113**, 7152–7167.
[84] Poirier, G. E., Tarlov, M. J., and Rushmeier, H. E., 1994, *Langmuir*, **10**, 3383–3386.
[85] Snyder, R. G., Strauss, H. L., and Elliger, C. A., 1982, *J. phys. Chem.*, **86**, 5145–5150.
[86] Terrill, R. H., Tanzer, T. A., and Bohn, P. W., 1998, *Langmuir*, **14**, 845–854.
[87] Wan, L. J., Terashima, M., Noda, H., and Osawa, M., 2000, *J. phys. Chem.*, **104**, 3563–3569.
[88] Zhang, Z. J., and Ima, T., 2001, *J. Colloid Interface Sci.*, **233**, 99–106.
[89] Resmi, M. R., and Pradeep, T., 2000, *J. mol. Spectrosc.*, **202**, 303–305.
[90] Moskovits, M., 1982, *J. chem. Phys.*, **77**, 4408–4416.
[91] Ruperez, A., and Laserna, J. J., 1996, Surface-enhanced raman spectroscopy, *Modern Techniques in Raman Spectroscopy*, edited by J. J. Laserna (Chichester: Wiley), p. 240.
[92] Bryant, M. A., and Pemberton, J. E., 1991, *J. Am. Chem. Soc.*, **113**, 8284–8293.
[93] Sandhyarani, N., and Pradeep, T., 1998, *Vacuum*, **49**, 279–284.
[94] Bryant, M. A., and Pemberton, J. E., 1991, *J. Am. Chem. Soc.*, **113**, 3629–3637.
[95] Lee, S. B., Kim, K., Kim, M. S., Oh, W. S., and Lee, Y. S., 1993, *J. mol. Struct.*, **296**, 5–13.
[96] Guyot-Sionnest, P., Hunt, J. H., and Shen, Y. R., 1987, *Phys. Rev. Lett.*, **59**, 1597–1600.
[97] Himmelhaus, M., and Buck, M., 2001, *J. Vac. Sci. Technol.* A, **19**, 2717–2736.
[98] Himmelhaus, M., Eisert, F., Buck, M., and Grunze, M., 2000, *J. phys. Chem.* B, **104**, 576–584.
[99] Humbert, C., Dreesen, L., Mani, A. A., Caudano, Y., Lemaire, J. J., Thiry, P. A., and Peremans, A., 2002, *Surf. Sci.*, **502**, 203–207.
[100] Zolk, M., Eisert, F., Pipper, J., Herrwerth, S., Eck, W., Buck, M., and Grunze, M, 2000, *Langmuir*, **16**, 5849–5852.
[101] Dreesen, L., Humbert, C., Hollander, P., Mani, A. A., Ataka, K., Thiry, P. A., and Peremans, A., 2001, *Chem. Phys. Lett.*, **333**, 327–331.
[102] Sellers, H., Ulman, A., Shnidman, Y., and Eilers, J. E., 1993, *J. Am. Chem. Soc.*, **115**, 9389–9401.
[103] Gronbeck, H., Curioni, A., and Anderoni, W., 2000, *J. Am. Chem. Soc.*, **122**, 3839–3842.
[104] Bain, C. D., Troughton, E. B., Tao, Y. T., Evall, J., Whitesides, M., and Nuzzo, R. G., 1989, *J. Am. Chem. Soc.*, **111**, 321–325.
[105] Jung, L. S., and Campbell, C. T., 2000, *Phys. Rev. Lett.*, **84**, 5164–5167.
[106] Karpovich, D. S., and Blanchard, G. J., 1994, *Langmuir*, **10**, 3315–3322.
[107] Zarnikov, M., Frey, S., Rong, H., Yang, Y-J., Heister, K., Buck, M., and Grunze, M., 2000, *Phys. Chem. chem. Phys.*, **2**, 3359–3362.

[108] Fenter, P., Eberhardt, A., Liang, K. S., and Eisenberger, P., 1997, *J. chem. Phys.*, **106**, 1600–1608.
[109] Eu, S., and Paik, W. K., 1999, *Mol. Cryst. Liq. Cryst.*, **337**, 49–52.
[110] Beena, G., Thomas, U., Sandhyarani, N., and Pradeep, T. (to be submitted).
[111] Thomas, R .C., Sun, L., Crooks, R. M., and Ricco, A. J., 1991, *Langmuir*, **7**, 7164.
[112] Jung, L.S., and Campbell, C.T., 2000, *J. phys. Chem.* B, **104**, 11168–11178.
[113] Bieubyck, H. A., Bain, C. D., and Whitesides, G. M., 1994, *Langmuir*, **10**, 1825–1831.
[114] Schreiber, F., Eberhardt, A., Leung, T. Y. B., Schwartz, P., Wetterer, S. M., Lavrich, D. J., Berman, L., Fenter, P., Eisenberger, P., and Scoles, G., 1998, *Phys. Rev.* B, **57**, 12476–12481.
[115] Eberhardt, A., Fenter, P., and Eisenberger, P., 1998, *Surf. Sci.*, **397**, L285–L290.
[116] Poirier, G. E., and Tarlov, M. J., 1994, *Langmuir*, **10**, 2853.
[117] Schonenberger, C., Sondaghuethorst, J. A. M., Jorritsma, J., and Fokkink, L. G. J., 1994, *Langmuir*, **10**, 611–614.
[118] Bucher, J. P., Santesson, L., and Kern, K., 1994, *Langmuir*, **10**, 979–983.
[119] Nemetz, A., Fischer, T., Ulman, A., and Knoll, W., 1993, *J. chem. Phys.*, **98**, 5912.
[120] Zharnikov, M., and Grunze, M., 2001, *J. Phys.: condens. Matter*, **13**, 11333–11365.
[121] Schoenfisch, M. H., and Pemberton, J. E., 1998, *J. Am. Chem. Soc.*, **120**, 4502.
[122] Zhang, Y., Terrill, R. H., Tanzer, T. A., and Bohn, P. W., 1998, *J. Am. Chem. Soc.*, **120**, 2654.
[123] Ulman, A., 1991, *Adv. Mater.*, **3**, 298–303.
[124] Chidsey, C. E. D., Liu, G.-Y., Rowntree, P., and Scoles, G., 1991, *J. chem. Phys.*, **94**, 8493–8502.
[125] Camillone III, N., Chidsey, C. E. D., Liu, G.-Y., Putvinski, T. M., and Scoles, G., 1991, *J. chem. Phys.*, **94**, 8493–8502.
[126] Nuzzo, R. G., Korenic, E. M., and Dubois, L. H., 1990, *J. chem. Phys.*, **93**, 767.
[127] Hautman, J., and Klein, M., 1990, *J. chem. Phys.*, **93**, 7483–7492.
[128] Mar, W., and Klein, M. L., 1994, *Langmuir*, **10**, 188–196.
[129] Hautman, J., and Klein, M., 1989, *J. chem. Phys.*, **91**, 4994–5001.
[130] Taut, C., Pertsin, A. J., and Grunze, M., 1996, *Langmuir*, **12**, 3481–3489.
[131] Bhatia, R., and Garrison, B. J., 1997, *Langmuir*, **13**, 765–769.
[132] Sadreev, A. F., and Sukhinin, Y. V., 1997, *J. chem. Phys.*, **107**, 2643–2652.
[133] Dubois, L. H., Zegarik, B. R., and Nuzzo, R. G., 1990, *J. Electron. Spectrosc. relat. Phenom.*, **54/55**, 1143–1152.
[134] Bensebaa, F., Ellis, T. H., Badia, A., and Lennox, R. B., 1995, *J. Vac. Sci. Technol.* A, **13**, 1331–1336.
[135] Bensebaa, F., Ellis, T. H., Badia, A., and Lennox, R. B., 1998, *Langmuir*, **14**, 2361–2367.
[136] Bensebaa, F., Ellis, T. H., Kruus, E., Voicu, R., and Zhou, Y., 1998, *Langmuir*, **14**, 6579–6587.
[137] Sandhyarani, N., Antony, M. P., Panneer Selvam, G., and Pradeep, T., 2000, *J. chem. Phys.*, **113**, 9794–9803.
[138] Voicu, R., Badia, A., Mrin, F., Lennox, R. B., and Ellis, T. H., 2001, *Chem. Mater.*, **13**, 2266–2271.
[139] Lee, S. J., Han, S. W., Choi, H. J., and Kim, K., 2001, *Eur. phys. J. D: at., mol. opt. Phys.*, **16**, 293–296.
[140] Teuscher, J. H., Yeager, L. J., Yoo, H., Chadwick, J. E., and Garrell, R. L., 1997, *Faraday Discuss.*, **107**, 399–416.
[141] Byloos, M., Al-Maznai, H., and Morin, M., 2001, *J. phys. Chem.* B., **105**, 5900–5905.
[142] Badia, A., Back, R., and Lennox, R. B., 1994, *Angew. Chem., int. Edn. Engl.*, **33**, 2332–2334.
[143] Gyepi-Garbrah, S. H., and Šilerová, R., 2001, *Phys. Chem. chem. Phys.*, **3**, 2117–2123.
[144] Venkataramanan, M., and Pradeep, T., 2000, *Anal. Chem.*, **72**, 5852–5856.
[145] Evans, S. D., Sharma, R., and Ulman, A., 1991, *Langmuir*, **7**, 156–161.

[146] Bucher, J.-P., Santesson, L., and Kern, K., 1994, *Langmuir*, **10**, 979–983.
[147] Delamarche, E., Michel, B., Kang, H., and Gerber, Ch., 1994, *Langmuir*, **10**, 4103–4108.
[148] Poirier, G. E., Fitts, W. P., and White, J. M., 2001, *Langmuir*, **17**, 1176–1183.
[149] Schmid, G., 1992, *Chem. Rev*., **92**, 1709–1727.
[150] Schmid, G., 2001, *Nanoscale Materials in Chemistry*, edited by K. J. Klabunde (New York: Wiley).
[151] Schön, G., and Simon, U., 1995, *Colloid Polym. Sci*., **273**, 101–117.
[152] Kang, S.Y., and Kim, K., 1998, *Langmuir*, **14**, 226–230.
[153] Vijaya Sarathy, K., Raina, G., Yadav, R. T., Kulkarni, G. U., and Rao, C. N. R., 1997, *J. phys. Chem.* B, **101**, 9876–9880.
[154] Shelley, E. J., Ryan, D., Johnson, S. R., Couillard, M., Fitzmaurice, D., Nellist, P. D., Chen, Y., Palmer, R. E., and Preece, J. A., 2002, *Langmuir*, **18**, 1791–1795.
[155] Shon, Y. S., Mazzitelli, C., and Murray, R. W., 2001, *Langmuir*, **17**, 7735–7741.
[156] Porter, L. A., Ji, D., Wescott, S. L., Graupe, M., Czernuszewicz, R. S., Halas, N. J., and Lee, T. R., 1998, *Langmuir*, **14**, 7378–7386.
[157] Chen, S., Templeton, A. C., and Murray, R. W., 2000, *Langmuir*, **16**, 3543–3548.
[158] Weisbecker, C. S., Merrit, M. V., and Whitesides, G. M., 1996, *Langmuir*, **12**, 3763–3772.
[159] Liu, J., Ong, W., Kaifer, A. E., and Peinador, C., 2002, *Langmuir*, **18**, 5981–5983.
[160] Maye, M. M., Zheng, W. X., Leibowitz, F. L., Ly, N. K., and Zhong, C. J., 2000, *Langmuir*, **16**, 490–497.
[161] Chaki, N. K., Sudrik, S. G., Sonawane, H. R., and Vijayamohanan, K., 2002, *Chem. Commun*., 76–77.
[162] Sánchez, L. R., Blanco, M. C., and López-Quintela, M. A., 2000, *J. phys. Chem.* B, **104**, 9683–9688.
[163] Zhu, J., Liu, S., Palchik, O., Koltypin, Y., and Gedanken, A., 2000, *Langmuir*, **16**, 6396–6399.
[164] Leff, D. V., Brandt, L., and Heath, J. R., 1996, *Langmuir*, **12**, 4723–4730.
[165] Vijaya Sarathy, K., Kulkarni, G. U., and Rao C. N. R., 1997, *J. Chem. Soc., chem. Commun*., 537–538.
[166] Chen, S., and Murray, R. W., 1999, *Langmuir*, **15**, 682–689.
[167] Grabar, C. C., Brown, K. R., Keating, C. D., Stranick, S. J., Tang, S.-L., and Natan, M. J., 1997, *Anal. Chem*., **69**, 471–477.
[168] Terril, R. H., Postlethwaite, T. A., Chen, C.-H., Poon, C.-D., Terzis, A., Chen, A., Hutchison, J. E., Clark, M. R., Wignall, G., Londono, J. D., Superfine, R., Falvo, M., Johnson, C. S., Samulski Jr, E. T., and Murray, R. W., 1995, *J. Am. Chem. Soc*., **117**, 12537–12548.
[169] Wang, B., Xiao, X., Huang, X., Sheng, P., and Hou, J. G., 2000, *Appl. Phys. Lett*., **77**, 1179–1181.
[170] Huang, S., Tsutsui, G., Sakaue, H., Shingubara, S., and Takahagi, T., 2000, *J. Vac. Sci. Technol. B: Microelectron. Nanometer Struct*., **18**, 2653–2657.
[171] Chen, S., Ingram, R. S., Hostetler, M. J., Pietron, J. J., Murray, R. W., Schaaff, T. G., Khoury, J. T., Alvarez, M., and Whetten, R. L., 1998, *Science*, **280**, 2098–2101
[172] Leff, D. V., Ohara, P. C., Heath, J. R., and Gelbart, W. M., 1995, *J. phys. Chem*., **99**, 7036–7041.
[173] Whetten, R. L., Shaffigullin, M. N., Khoury, J. T., Schaaf, T. G., Vezmar, I., Alvarez, M. M., and Wilkinson, A., 1999, *Acc. chem. Res*., **32**, 397–406.
[174] West, A. R., 1987, *Solid State Chemistry and its Applications* (New York: Wiley).
[175] Zanchet, D., Hall, B. D., and Ugarte, D., 2000, *J. phys. Chem.* B, **104**, 11013–11018.
[176] Wang, Z. L., 1998, *Adv. Mater*., **10**, 13–30.
[177] Korgel, B. A., and Fitzmaurice, D., 1999, *Phys. Rev.* B, **59**, 14191–14201.
[178] Sandhyarani, N., Resmi, M. R., Unnikrishnan, R., Vidyasagar, K., Ma, S., Antony, M. P., Selvam, G. P., Visalakshi, V., Chandrakumar, N., Pandian, K., Tao, Y.-T., and Pradeep, T., 2000, *Chem. Mater*., **12**, 104–113.

[179] Cleveland, C. L., Landman, U., Schaaff, T. G., Shafigullin, M. N., Stephens, P. W., and Whetten, R. L., 1997, *Phys. Rev. Lett.*, **79**, 1873–1876.
[180] Zanchet, D., Tolentino, H., Alves, M. C. M., Alves, O. L., and Ugarte, D., 2000, *Chem. Phys. Lett.*, **323**, 167–172.
[181] Schaaff, T. G., Shafigullin, M. N., Khoury, J. T., Vezmar, I., and Whetten, R. L., 2001, *J. Phys. Chem.* B, **105**, 8785–8796.
[182] Arnold, R. J., and Reilley, J. P., 1998, *J. Am. Chem. Soc.*, **120**, 1528–1532.
[183] Murthy, S., Bigioni, T. P., Wang, Z. L, Khoury, J. T., and Whetten, R. L., 1997, *Mater. Lett.*, **30**, 321–325.
[184] Wuelfing, W. P., Templeton, A. C., Hicks, J. F., and Murray, R. W., 1999, *Anal. Chem.*, **71**, 4069–4074.
[185] Wuelfing, W. P., Green, S. J., Pietron, J. J., Cliffel, D. E., and Murray, R. W., 2000, *J. Am. Chem. Soc.*, **122**, 11465–11472.
[186] Bethel, D., Brust, M., Schiffrin, D. J., and Kiely, C., 1996, *J. electroanal. Chem.*, **409**, 137–143.
[187] Fishelson, N., Shkrob, I., Lev, O., Gun, J., and Modestov, A. D., 2001, *Langmuir*, **17**, 403–412.
[188] Link, S., and El-Sayed, M. A., 1999, *J. phys. Chem.* B, **103**, 8410–8426.
[189] Henglein, A., 1993, *J. phys. Chem.*, **97**, 5457–5471.
[190] Templeton, A. C., Pietron, J. J., Murray, R. W., and Mulvaney, P., 2000, *J. phys. Chem.* B, **104**, 564–570.
[191] Sun, Y., and Xia, Y., 2002, *Anal. Chem.*, **74**, 5297–5305.
[192] Pham, T., Jackson, B., Halas, N. J., and Lee, T. R., 2002, *Langmuir*, **18**, 4915–4920.
[193] He, S., Yao, J., Jiang, P., Shi, D., Zhang, H., Xie, S., Pang, S., and Gao, H., 2001, *Langmuir*, **17**, 1571–1575.
[194] Malinsky, M. D., Kelly, K. L., Schatz, G. C., and Van Duyne, R. P., 2001, *J. Am. Chem. Soc.*, **123**, 1471–1482.
[195] Bourg, M. C., Badia, A., and Lennox, R. B., 2000, *J. phys. Chem.* B, **104**, 6562–6567.
[196] Bensebaa, F., Yu, Z., Deslandesa, Y., Kruus, E., and Ellis, T. H., 1998, *Surf. Sci.*, **405**, L472–L 476.
[197] Luedtke, W. D., and Landman, U., 1996, *J. phys. Chem.*, **100**, 13323–13329.
[198] Van Hyning, D. L., Klemperer, W. G., and Zukoski, C. F., 2001, *Langmuir*, **17**, 3128–3135.
[199] Hostetler, M. J., Stokes, J. J., and Murray, R. W., 1996, *Langmuir*, **12**, 3604–3612.
[200] Badia, A., Denners, L., Dickinson, L., Morin, F. G., Lennox, R. B., and Reven, L., 1997, *J. Am. Chem. Soc.*, **119**, 11104–11105.
[201] Wang, B., Wang, H. Q., Li ,H. X., Zeng, C. G., Hou, J. G., Xiao, X. D., 2001, *Phys. Rev.* B, **63**, art.no.035403-1–035403-7.
[202] Thomas, P. J., Kulkami, G. U., and Rao, C. N. R., 2000, *Chem. Phys. Lett.*, **321**, 163–168.
[203] Hasan, M., Bethell, D., and Brust, M., 2002, *J. Am. Chem. Soc.*, **124**, 1132–1133.
[204] Storhoff, J. J., Lazarides, A. A., Mucic, R. C., Mirkin, C. A., Letsinger, R. L., and Schatz, G. C., 2000, *J. Am. Chem. Soc.*, **122**, 4640–4650.
[205] Luedtke, W. D., and Landman, U., 1998, *J. phys. Chem.* B, **102**, 6566–6572.
[206] Badia, A., Singh, S., Demers, L., Cuccia, L., Brown, G. R., and Lennox, R. B., 1996, *Chem. Eur. J.*, **2**, 359–363.
[207] Badia, A., Cuccia, L., Demers, L., Morin, F., and Lennox, R. B., 1997, *J. Am. Chem. Soc.*, **119**, 2682–2692.
[208] Badia, A., Gao, W., Singh, S., Demers, L., Cuccia, L., and Reven, L., 1996, *Langmuir*, **12**, 1262–1269.
[209] Schmitt, H., Badia, A., Dickinson, L., and Lennox, R. B., 1998, *Adv. Mater.*, **10**, 475–480.
[210] Snyder, R. G., 1961, *J. mol. Spectrosc.*, **7**, 116–144.
[211] Dubois, L. H., and Nuzzo, R. G., 1992, *Annu. Rev. phys. Chem.*, **43**, 437–463.
[212] Wang, Z. L., 2000, *J. phys. Chem. B*, **104**, 1153–1175.
[213] Bee, M., 1988, *Quasielastic Neutron Scattering* (Bristol: Hilger).

[214] Mitra, S., Nair, B., Pradeep, T., Goyal, P. S., and Mukhopadhyay, R., 2002, *J. Phys. Chem.* B, **106**, 3960–3967.
[215] Mukhopadhyay, R., Mitra, S., Nair, B., Pradeep, T., Tsukushi, T., and Ikeda, S., *J. Chem. Phys.* (in press).
[216] Sandhyarani, N., and Pradeep, T., 2001, *Chem. Phys. Lett.*, **338**, 33–36.
[217] Sandhyarani, N., Pradeep, T., and Fransisco, J. S., 2001, *Chem. Phys. Lett.*, **342**, 272–276.
[218] Sreekumaran Nair A., and Pradeep, T. (submitted).
[219] Wuelfing, W. P., Zamborini, F. P., Templeton, A. C., Wen, X., Yoon, H., and Murray, R. W., 2001, *Chem. Mater.*, **13**, 87–95.
[220] Schaaff, T. G., and Whetten, R. L., 1999, *J. phys. Chem.* B, **103**, 9394–9396.
[221] Ah, C. S., Han, H. S., Kim, K., and Jang, D. J., 2000, *Pure appl. Chem.*, **72**, 91–99.